Peroxisomal import is circadian in glia and regulates sleep and lipid metabolism

Anurag Das[1,2,8]*, Irma Magaly Rivas-Serna[3], Marlene Dorneich-Hayes[1,4], Ankur Kumar[1,4], Lakpa Sherpa[1,4], Ruiqi Liu[1, 5], Kerui Huang[1,7], Vera Mazurak[3], John P. Vaughen[6]*, Hua Bai[1]*

1 Department of Genetics, Development, and Cell Biology, Iowa State University, Ames, IA 50011, USA
2 Interdepartmental Neuroscience PhD program, Iowa State University, Ames, IA 50011, USA
3 Department of Agriculture, Food, and Nutritional Science, University of Alberta; Edmonton, T6G 2R3, Canada.
4 Interdepartmental Genetics & Genomics PhD program, Iowa State University, Ames, IA 50011, USA
5 Interdepartmental MCDB PhD program, Iowa State University, Ames, IA 50011, USA
6 Department of Anatomy, University of California San Francisco, San Francisco, CA 94143, USA
7 Present address: Department of Genetics, Blavatnik Institute, Harvard Medical School, Boston, MA 02115, USA
8 Lead Contact
*Authors for correspondence: Anurag Das (anuragd7@iastate.edu), John P. Vaughen (john.vaughen@ucsf.edu), Hua Bai (hbai@iastate.edu)

Abstract

Peroxisomes are critical organelles that detoxify cellular waste while also catabolizing and anabolizing lipids. How peroxisomes coordinate protein import and support metabolic functions across complex tissues and timescales remains poorly understood *in vivo*. Using the *Drosophila* brain, we discover a striking enrichment of peroxisomes in the neuronal soma and the cortex glia that enwrap them. Unexpectedly, import of peroxisomal proteins into cortex glia, but not neurons, oscillated across time and peaked in the early morning. Rhythmic peroxisomal import in cortex glia autonomously required the circadian clock and Peroxin 5 (Pex5; peroxisomal biogenesis factor 5 homolog), with import persistently elevated in clock mutants. Notably, reducing *Pex5* in cortex glia, but not neurons, caused hyperactivity and reduced total sleep. Moreover, brain lipid metabolism was dramatically altered upon *Pex5* knockdown, with glia impacting sphingolipids and triacylglycerols, and neurons impacting phospholipids. The cell-type specificity of these Pex5 phenotypes highlights unique roles for peroxisomal import in both sleep and lipid metabolism in the brain.

Introduction

Peroxisomes are responsible for vital metabolic activities ranging from lipid metabolism by beta-oxidation and ether lipid biosynthesis[1],[2],[3] to reactive oxygen species detoxification[4],[5],[6]. Accordingly, mutations afflicting peroxisomes can cause

numerous diseases, including Zellweger Syndrome[7],[8], a severe peroxisomal biogenesis disorder stemming from mutations in one of the 12 different PEX genes in humans[9]. While these diseases often manifest in the brain[10],[11],[12], why these diseases occur and how peroxisomes are regulated across diverse brain cells and timescales remains incompletely understood.

Peroxisomes require a unique import machinery capable of translocating fully folded and oligomeric substrates from the cytosol into the peroxisomal matrix (lumen)[13]. The Peroxin-5 protein Pex5 is a vital cog in this translocation machinery, as it functions as a major receptor for targeting proteins to the peroxisomal matrix by the peroxisomal targeting signal 1, or PTS1 (e.g. Ser-Lys-Leu, SKL)[14],[15],[16]. Notably, loss of Pex5 from *Drosophila* to mice and humans causes severe defects, including motor and cognitive decline simultaneously with demyelination, axonal loss, and gliosis[17]. While *Pex5* mutants are lethal[18], *Pex5* disruption selectively in mouse oligodendrocytes caused pronounced neurological and lipidomic defects[5]. In contrast, neuronal or astrocytic *Pex5* disruption led to mild defects[17]. While peroxisomal import may thus have cell-type specific effects in the brain, this has not been systematically explored.

Drosophila is an outstanding genetic model to interrogate peroxisomes and peroxisomal import function in the brain, given the capability to genetically track and manipulate peroxisomal import in a cell-type specific manner. The fly brain harbors a diversity of glial subtypes and neurons thought to share homologous functions with mammalian counterparts including astrocytes and microglia[19–23]. For example, neuronal synaptic processes are tiled by astrocyte-like glia in mammals[24] and insects[25], and fly axons are isolated and insulated by ensheathing (CNS) and wrapping glia (PNS), analogous to oligodendrocytes and Schwann cells[23,26,27]. In mammals, satellite glia enwrap single neuronal soma[28], while in adult flies, cortex glia encompass dozens of neuronal soma in a honeycombed morphology, and accordingly regulate neuronal activity among other functions[22],[29],[30],[31],[32],[33],[19].

Alongside functionally homologous glia, flies also display complex behavioral repertoires ranging from memory to sleep[34],[35],[36],[37],[38] . While all behavior is tightly coordinated by rhythmic changes experienced under the shared 24-hour light/dark cycle[39],[40] , in complex metazoan brains the clock is controlled by a network of circadian pacemaker neurons [41],[42],[43],[44],[45],[46],[47]. Within these cells, negative transcriptional feedback loops between Period (Period/PER), Clock (Clock/CLK), and Cycle (cyc/BMAL1) enforce a ~24hour molecular rhythm[48]. Glia also express core circadian clock machinery and can modulate sleep through myriad pathways, including remodeling neuronal synapses and regulating metabolism[41,49–51]. Moreover, autonomous disruption of glial clocks directly disrupts sleep and circadian plasticity in clock pacemaker neurons in flies[44]. Although circadian rhythms govern metabolic homeostasis across organisms[52],[53],[54] and in diseases[55], how subcellular organelle dynamics in glia and neurons change across time remains underexplored.

Here, we tested how peroxisomal import is coordinated in the fly brain in a cell-type specific manner. We discovered that cortex glia are hubs of abundant matrix peroxisomal proteins and high peroxisomal import, in contrast to other brain glia. Moreover, peroxisomal import in cortex glia but not neurons varied dramatically over circadian time, with elevated import in the early morning. Through genetic analyses, we determined that Pex5 and the core circadian clock autonomously regulates oscillatory peroxisomal import in cortex glia. Notably, loss of Pex5 in cortex glia disrupted sleep behavior and caused ectopic lipid droplets, while loss of Pex5 in all glia or all neurons profoundly altered multiple lipid classes. Together, our work identifies circadian fluctuations in peroxisomal import to specialized glia, which require Pex5 for sleep behavior, and highlights cell-type specific roles of Pex5 in brain lipid metabolism.

Results

105 **Peroxisomal abundance and import are enriched in neurons and cortex glia**

106 Peroxisomal import (Figure 1A) is the active translocation of matrix proteins from the
107 cytosol into the peroxisomal lumen via the canonical peroxisomal targeting signal 1
108 (PTS1; the most common consensus tripeptide sequence is Serine-Lysine-Leucine,
109 SKL). These sequences are recognized by the cytosolic import receptor Pex5, which
110 facilitates shuttling by releasing imported cargo in the peroxisomal lumen[56]. We first
111 sought to survey peroxisomal import in the adult CNS by co-staining for the peroxisomal
112 marker PMP70 (Peroxisomal membrane protein 70)[57],[16],[58],[59] and *UAS-*
113 *eYFP.PTS1*[60], which revealed cell-type specific patterns of peroxisomal import when
114 crossed to GAL4 driver lines targeting major CNS populations (Figure 1B). Both pan-glial
115 (*repo-GAL4*) and pan-neuronal (*nSyb-GAL4*) drivers expressed PTS1 puncta that
116 colocalized with PMP70 (Figure 1C). Notably, PMP70 was enriched at the cortex in pan-
117 glial experiments, suggesting that cortex glia may have particularly high levels of
118 peroxisomal import. Indeed, by genetically tracking peroxisomal import with *UAS-*
119 *eYFP.PTS1* across different glial subtypes, we found that PTS1+,PMP70+ puncta were
120 most abundant in cortex glia compared to other glial classes (Figure 1D-F; Figure S1A-
121 D). Thus, among the CNS glia, cortex glia have uniquely heightened peroxisomal import.

122 **Peroxisomal import oscillates in cortex glia across time and requires Pex5**

123 While further characterizing peroxisomal import, we made the serendipitous finding that
124 import fluctuated across circadian time in cortex glia but not neurons (Figure 2A-B; Figure
125 S2I-K; Zeitgeber 0 (ZT0) denotes lights-on). While neurons had consistently high levels
126 of PTS1 that colocalized with PMP70, cortex glia had three-fold higher levels of PTS1 at
127 ZT2 and ZT4 (Figure S2I-K) compared to a nadir at ZT8 (Figure 2C-F; Pearson decreases
128 from 0.6 to 0.2, while PTS1 puncta number decreases from 28 to 8). A similar enrichment
129 of morning import was observed with an anti-SKL antibody (Figure S2B-D). Import
130 oscillations also occurred under constant darkness implicating endogenous clock control
131 (Figure 2G-J; Figure S2L-N). While cortex glia PTS1 puncta remained low in the evening,
132 the colocalization between PTS1 and PMP70 at ZT14 was higher than at ZT8 (Figure
133 2C), and we often observed diffuse PTS1 membranous signals at ZT14 (Figure S2E).

134 Intrigued, we tested whether the central regulator of peroxisomal import, Pex5 (Figure
135 1A), also oscillated in the brain. We used CRISPR to generate a knock-in FLAG tag into
136 the endogenous Pex5 locus (Figure 2K; Figure S2G and see Methods). Importantly,
137 *Pex5.FLAG* flies were viable and healthy (Figure S2F-F'), unlike Pex5 loss-of-function
138 alleles, which are lethal[18]; we did note a reduction in the *Pex5.FLAG* transcript as
139 compared to endogenous *Pex5* by full animal qRT-PCR (Figure S2H), suggesting that
140 the FLAG tag could possibly create a hypomorphic allele. Using *Pex5.*FLAG, we observed
141 that Pex5 protein robustly oscillated across time in the brain under light-dark and dark-
142 dark conditions, peaking at ZT2 during the height of PTS1 import in cortex glia (Figure
143 2L-O; Figure S2A; note that the majority of Pex5 is expected to be cytosolic). Moreover,
144 this oscillatory signature is present in single cell RNA sequencing data, where transcripts
145 of *Pex5*, *Pex11*, and the peroxisome proliferator-activated receptor (PPAR) homolog
146 *Eip75B* peak at similar times in cortex glia[43] (Figure S3 A-B). To test if Pex5 is obligatory
147 for basal levels of peroxisomal import in glia, we knocked-down *Pex5* using an *RNAi* that
148 reduces *Pex5* transcripts by over 50% [4]. $Pex5^{KD}$ specifically in cortex glia strongly
149 suppressed overall peroxisomal import, with reduced PTS1 puncta that no longer
150 oscillated across time, but did not alter PMP70+ puncta (Figure 2P-T). This phenotype
151 was replicated with a second Pex5 *RNAi* line (Figure S4A-D). Thus, in cortex glia,
152 peroxisomal import and Pex5 levels are highest in the morning, and oscillations in
153 peroxisomal import require Pex5.
154
155 **The circadian clock autonomously controls peroxisomal import in cortex glia**
156
157 To test if the circadian clock regulated peroxisomal import, we utilized *period* arrhythmic
158 mutants (per^{01}), and measured PTS1 import in cortex glia at the apex (ZT2) and nadir
159 (ZT8) of import. Strikingly, *per* mutants had persistently elevated PTS1 import in cortex
160 glia (Figure 3A-E). As all glia and subsets of neurons express the core circadian clock
161 machinery[61],[62],[63],[64],[65],[43], we next investigated whether cortex glia
162 autonomously require a functioning circadian clock by leveraging a dominant-negative
163 Clock transgene[66] ($UAS\text{-}Clk^{DN}$) or a validated *per RNAi line* [67],[68,69]. In both
164 manipulations, autonomously disrupting the cortex glia circadian clock triggered aberrant

165 and persistently elevated levels of PMP70/SKL at ZT8 (Figure 3F-J; Figure S6A-E).
166 Additionally, removing the PPAR homolog and downstream target of Per, *Eip75B*, in
167 cortex glia phenocopied the effects of *per* and Clk^{DN} and persistently elevated import
168 (Figure S5A-C).To test if Pex5 functioned downstream of the clock, we overexpressed
169 Pex5 in per^{KD} cortex glia via the CRISPR/Cas9 transcriptional activation system[70].
170 Surprisingly, Pex5 overexpression in per^{KD} cortex glia normalized import at ZT8 (Fig. S6F-
171 J). Thus, the circadian clock and Pex5 autonomously control rhythmic peroxisomal import
172 into a specialized subset of brain cells, the cortex glia.
173
174 **Loss of *Pex5* selectively in cortex glia disrupts sleep**
175
176 Given the striking circadian oscillations in peroxisomal import in cortex glia, and that
177 cortex glia regulate sleep behavior[71],[72], we next examined whether removing *Pex5* in
178 different cells altered sleep. Remarkably, disrupting *Pex5* in cortex glia reduced both
179 daytime and nighttime sleep, with shorter sleep bout duration (Figure 4A-D). This
180 phenotype likely stems from hyperactivity, as total daytime activity was elevated in $Pex5^{KD}$
181 flies (Figure 4E-G). Similar deficits occurred under constant darkness (Figure 4H-N), and
182 there were no clear defects in sleep latency or circadian rhythmicity (Figure S7A-B). In
183 contrast, knocking-down *Pex5* in ensheathing glia had no impact on daytime sleep and
184 modest effects on nighttime sleep (Figure S7K-R). Similarly, removing *Pex5* from neurons
185 with *nSyb-GAL4* did not consistently affect daytime or nighttime sleep (Figure S7C-J).
186 Thus, Pex5 plays a critical, cell-type specific role in cortex glia that regulates activity and
187 total sleep.
188
189 **Pex5 is essential for lipid homeostasis in the adult brain**
190
191 Intriguingly, wakefulness causes accumulation of lipid droplets in cortex glia and
192 ensheathing glia[72], and peroxisomes and peroxins[73] can directly interact with lipid
193 droplets (LD), with Pex5 stimulating lipolysis[74]. We thus hypothesized that removing
194 *Pex5* would alter lipid metabolism in the brain. Indeed, knockdown of *Pex5* in cortex glia
195 dramatically increased lipid droplet number and size (Figure 5A-C) with lipid droplets

196 appearing adjacent to PMP70 puncta. Knocking down Pex5 in neurons moderately
197 increased lipid droplet number and size (Figure S8J-L). These data are consistent with
198 Pex5 function impacting lipid droplet biology, either through peroxisomal import or direct
199 effects on lipolysis through lipase recruitment [74].
200
201 We next used liquid chromatography-tandem mass spectrometry (LC-MS/MS) for
202 targeted analyses of *Drosophila* sphingolipids (SL), phospholipids (PL; including
203 glycerophospholipids and alky-ether phospholipids); free fatty acids; and triacylglycerols
204 (TAG). We dissected brains from controls (*RNAi* and *GAL4* lines separately), or flies with
205 *Pex5* knocked-down in all glia (*repo-GAL4* > *Pex5*^{KD}) or all neurons (*nSysb-GAL4* >
206 *Pex5*^{KD}*)* at ZT10-12 in day 7 adults. Both neuronal or glial removal of *Pex5* caused
207 dramatic and unique shifts to the global brain lipidome (Figure 5D-E), with more species
208 altered by the glial manipulation, including decreases to individual and total TAGs (Figure
209 5D; Figure S8A-B). Although aged *Pex5* mutants accumulate very long chain fatty acids
210 (VLCFA) from impaired beta-oxidation, in young day 7 adults we did not detect
211 pronounced VLCFA accumulation in either glial or neuronal *Pex5*^{KD} (Figure S8C).
212 Strikingly, glial *Pex5*^{KD} significantly and specifically altered major ceramide
213 phosphoethanolamine (CPE) species by decreasing d14 sphingoid bases (d14; long-
214 chain base) and increasing d16 sphingoid bases (Figure 5G). This lipidomic signature
215 also occurs upon the glial disruption of serine palmitoyltransferase activity (*lace*^{KD}) [75],
216 suggesting that *de novo* sphingolipid biosynthesis may be impaired when glia lose Pex5 .
217 Interestingly, both glial and neuronal *Pex5*^{KD} brains had small but significant increases in
218 species bearing very long chain fatty acids (>C20) (Figure 5H).
219
220 In contrast to the sphingolipid defects triggered by glial *Pex5*^{KD}, neuronal *Pex5*^{KD} caused
221 a phospholipid defect characterized by increases in 18:3(omega-3/ω3) bearing fatty-acyl
222 chains in phosphatidylethanolamines (PE) and phosphatidylcholines (PC) (Figure 5I-J),
223 whereas phosphatidylinositols and phosphatidylserines were not affected (Figure S8D).
224 Intriguingly, PE increased following *Pex5* loss in oligodendrocytes, likely in compensation
225 for decreased ether phospholipids[5]. However, we did not detect major changes to alky-

226 ether phospholipids[76] in neuronal *Pex5*^{KD} (Figure S8E), but cannot exclude changes to
227 species not scanned.
228
229 Lastly, we also profiled cortex glia *Pex5*^{KD} brains by LC-MS/MS (Figure S8F-G), and
230 found modest effects on the global brain lipidome, with weak separation of samples by
231 principal component analysis for TAG, SL, and PL lipids (Figure S8I). In contrast to the
232 pan-glial loss of *Pex5,* cortex glial *Pex5*^{KD} did not severely reduce d14/d16 sphingolipid
233 ratios, and instead elevated two CPE species (Figure S8H; CPE d14:1/18:0 and
234 d14:2/18:0). These changes are unlikely to account for the lipid droplet phenotype, which
235 may be driven by neutral lipids not included in the scan (i.e., sterol esters). Taken
236 together, these data show that manipulating peroxisomal import in neurons or glia causes
237 strong and distinct phenotypes on the global brain lipidome.
238
239
240 **Discussion**
241
242 Here, we uncover circadian regulation of glial peroxisomal dynamics and link clock-
243 controlled organelle biology to brain-wide lipid metabolism and sleep behavior. By
244 systematic profiling of peroxisomal import in the brain, we elucidate that cortex glia have
245 enriched and dynamic peroxisomal import early in the morning. The circadian clock and
246 Pex5 autonomously control circadian import into cortex glia, and cortex glial Pex5 is
247 essential for preventing lipid droplet accumulation and sleep loss. Moreover, glial Pex5
248 is critical for TAG and sphingolipid homeostasis, whereas neuronal Pex5 was critical for
249 specific glycerophospholipids, highlighting cell-type specific outcomes of peroxisomal
250 import loss in the brain.
251
252 ***An evolutionarily conserved role for Pex5 in glia***

253 Prior investigations discovered key roles for Pex5 in oligodendrocytes[5] and Schwann
254 cells[6], with severe neurodegeneration and demyelination in *Pex5*^{KO} oligodendrocyte,
255 and nonautonomous effects on ion channel distribution downstream of lysosomal
256 dysfunction in Schwann cell *Pex5*^{KO}. In contrast, *Pex5*^{KO} neurons and astrocytes did not

257 cause overt pathology[17]. By tracking peroxisomal import and conducting *Pex5*
258 knockdown experiments across diverse brain cells, we found that cortex glia are
259 selectively enriched for Pex5-dependent circadian peroxisomal import. Thus, in both flies
260 and humans, glia play a central role in peroxisome-mediated processes, and circadian
261 peroxisomal import should be investigated in mammalian glia which similarly enwrap
262 neuronal soma. Homologues of the cortex glia based on structural morphology include
263 satellite glia cells, protoplasmic astrocytes, and perineuronal
264 oligodendrocytes[77],[78],[79],[80]. Notably, cortex glia extend fine membrane processes
265 tiling dozens of neuronal cell soma, regulate neruonal activity[29],[31], and serve as
266 reservoirs of energy and neutral lipids during development[81],[33] and adulthood[82].
267 Due to the close association of cortex glia with the neuronal cell soma, we speculate that
268 peroxisomes are vital to neuronal homeostasis through metabolic and cellular detoxifying
269 functions[83],[84],[29] . While we could not detect major lipid changes using LC-MS/MS
270 upon cortex glial *Pex5*^{KD}, this may be due to the manipulation targeting ~2% of the total
271 brain[85]. In contrast, pan-glial *Pex5*^{KD} severely depleted TAGs and altered sphingolipid
272 profiles, pointing to important roles for glial peroxisomal import in overall brain lipid
273 metabolism. Future work should determine more precisely how circadian peroxisomal
274 import by cortex glial regulates glial and neuronal metabolism and function.
275
276 ***Circadian control of peroxisomal import in cortex glia***
277
278 Circadian clocks regulate daily rhythms in organelle dynamics[52],[86], lipid
279 metabolites[87],[88],[89], and transcriptomes in various
280 tissues[90],[91],[92],[93],[94],[95],[96] . Our work raises the critical question of how
281 pervasively peroxisomal proteins and functions vary across circadian time. While we
282 demonstrate that Pex5 and peroxisomal import peak early in the morning at ZT2 and have
283 a trough at ZT8, future studies should test if all or subsets of peroxisomal proteins are
284 similarly circadian in cortex glia. Surprisingly, despite neurons containing high levels of
285 peroxisomal matrix proteins and PTS1 puncta, we did not detect variations in import
286 across time. Why do cortex glia undergo circadian peroxisomal import? The afternoon
287 cessation of peroxisomal import at ZT8 could suggest a restorative break, as ZT8 aligns
288 with an afternoon siesta thought to adjust for the hottest time of the day[97]. These

289 restorative breaks may be essential for clearing damaged peroxisomes or for timing lipid
290 metabolic loops. However, import does not correlate with activity, arguing against a direct
291 correlation between sleep pressure and peroxisomal import. An alternative hypothesis
292 would be a division of labor in the peroxisome, where at certain times of day specific
293 functions like detoxification or lipid metabolism are favored by enhanced import via Pex5.

294 While we link the circadian clock to glial peroxisomal import, *period* mutant larval fat
295 bodies have ultradian variation in lipid metabolism and peroxisomal import and
296 biogenesis[98], suggesting both clock and non-clock based mechanisms at play.
297 Intriguingly, a putative deubiquitinase for Pex5, USP2, shows circadian fluctuations in
298 localization to the peroxisome in liver that depend on the core clock[99], and a similar
299 mechanism may regulate the stability and activity of Pex5 in cortex glia.

300 ***Glial peroxisomes in sleep, neurodegeneration and lipid homeostasis***

301 Zellweger spectrum diseases[100],[101] are a group of heterogenous mutations in
302 peroxisomal proteins that cause neurodevelopmental and neurodegenerative
303 disorders.[102] As cortex glial Pex5 is essential for sleep and subject to circadian
304 regulation, it may be fruitful to investigate for circadian modulation of Zellweger disorder
305 phenotypes, including sleep. Our behavioral findings suggest a model wherein cortex glial
306 communicate with closely associated neuronal soma to regulate behavioral processes
307 such as sleep [103],[104]. Sleep deprivation induces a cytokine storm[105], and *Pex5*
308 perturbation also induces pro-inflammatory cytokine *upd3* in glial cells[4]. In flies, altered
309 lipid droplet metabolism in cortex and ensheathing glia downstream of neuronal oxidative
310 stress can cause sleep defects[72]. Moreover, a recent preprint reports that sleep itself
311 can control peroxisomal abundance and downstream oxidative damage in neurons [106].
312 Given that *Pex5* knockdown in cortex glia caused sleep loss and increased lipid droplets,
313 we speculate that neurons in aged $Pex5^{KD}$ flies could accumulate reactive oxygen species
314 and upregulate cytokines through metabolic coupling between neurons and glia.

315 Knockdown of Pex5 caused cell type-specific alterations to the young adult brain
316 lipidomes, arguing that peroxisomes serve different metabolic functions in neurons
317 (phospholipid homeostasis) versus glia (sphingolipid and TAG metabolism). The broad
318 loss of TAG upon glial knockout may occur from increased lipolysis of lipid droplets[107]

319 and/or decreased neutral lipid uptake and storage, which could be direct or secondary
320 effects of Pex5 depletion. Enhanced lipolysis may reflect a shifting energy balance of glial
321 cells with compromised peroxisomal import, and glial mitochondrial beta-oxidation is a
322 key determinant of both fly viability and TAG and lipid droplet abundances[108] . Prior
323 work on global *pex2, pex3,* and *pex16* mutants also observed changes in sphingolipid
324 homeostasis[109],[110]. The surprising phenotypic overlap of decreased d14, and
325 increased d16, sphingolipids in glial *Pex5* knockdown (Figure 6D-H) and glial knockdown
326 of *lace*, the rate limiting enzyme in sphingolipid biosynthesis, suggests that *Pex5* deficient
327 glia are defective in *de novo* sphingolipid biosynthesis. Whether this effect is primary
328 (defects in fatty acid substrates) or secondary (compromised glial health) remains to be
329 determined. Lastly, we were surprised to observe higher n-3 phosphatidylethanolamines
330 in neuronal *Pex5* knockdown brains, given that Zellweger patients often lose n-3
331 glycerophospholipids[111]. While our data point to important roles for neuronal
332 peroxisomes in phospholipid metabolism, future work is required to decipher the cause,
333 and consequences, of these lipid alterations.

334 In conclusion, by studying Pex5 in the adult *Drosophila* brain and the dynamics of
335 peroxisomal import, we identify extensive cell-type specific variability, with elevated
336 import in neurons and cortex glia. In cortex glia, import and Pex5 levels are under strict
337 circadian control. Our identification of sleep disruption upon Pex5 loss in cortex glia opens
338 the avenue to a deeper understanding of peroxisome function in the brain, and the
339 neurological consequences of peroxisomal disorders.
340
341
342
343
344
345
346
347
348
349

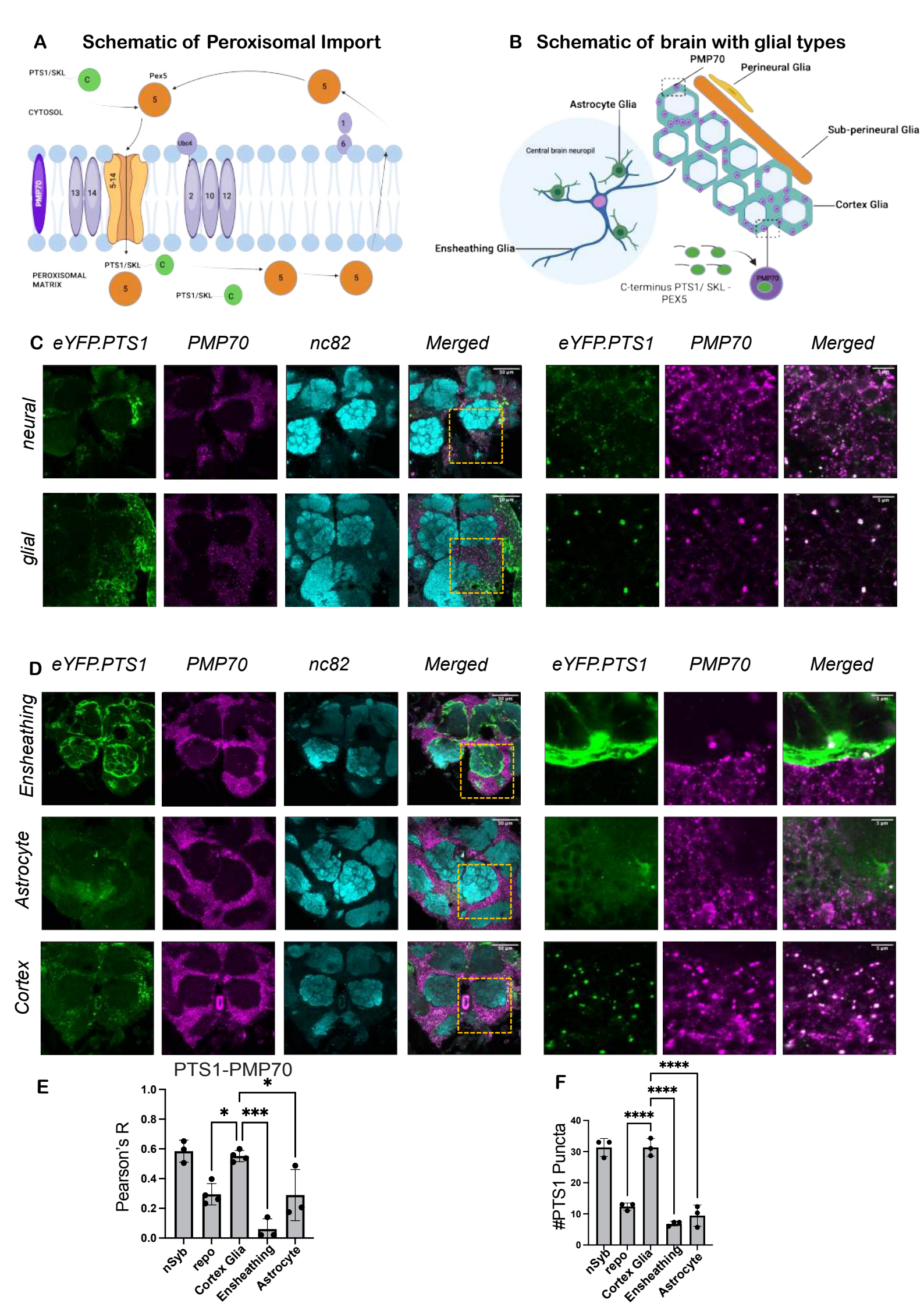
A
Schematic of Peroxisomal Import
PTS1/SKL
Pex5
CYTOSOL
Ubc4
PMP70
PEROXISOMAL MATRIX
B
Schematic of brain with glial types
PMP70
Perineural Glia
Astrocyte Glia
Sub-perineural Glia
Central brain neuropil
Cortex Glia
Ensheathing Glia
C-terminus PTS1/ SKL - PEX5
C
eYFP.PTS1
PMP70
nc82
Merged
neural
glial
D
Ensheathing
Astrocyte
Cortex
E
PTS1-PMP70
Pearson's R
nSyb
repo
Cortex Glia
Ensheathing
Astrocyte
F
#PTS1 Puncta

Figure 1. Peroxisomal abundance and import are enriched in neurons and cortex glia

(A) Schema of peroxisomal import machinery mediated by Pex5, the cytosolic import receptor that recognizes a *PTS1-SKL* harboring matrix protein and permits its active translocation from the cytosol to the peroxisomal lumen; Adapted from [15] and [56].

(B) Schematic of different glial cell types in the *Drosophila* central nervous system.

(C) Adult female *Drosophila* brains (7 days old) tracking peroxisome import in neurons with *UAS-eYFP.PTS1* using the pan-neural driver *nSyb-GAL4* or the pan-glial driver *repo- GAL4*. eYFP-tagged *PTS1*-protein import (green) is counterstained with PMP70 (magenta), an abundant peroxisomal membrane protein, and the pre-synaptic active zone protein bruchpilot (cyan; nc82). Yellow rectangle denotes area used for zooms into cortex below the antennal lobes and above the suboesophageal ganglion. Scale bars = 50μm and 5μm (zoom).

(D) Adult female *Drosophila* brains (7 days old) tracking peroxisomal import in glia subtypes using *UAS-eYFP.PTS1* (green) driven by *GMR56F03*-GAL4 (Ensheathing glia), *GMR83E10-GAL4* (Astrocyte-like glia), and cortex glia (*GMR54H02*-GAL4), counterstained with PMP70 (magenta) and nc82 (cyan). Yellow rectangle denotes area used for zooms into cortex below the antennal lobes and above the suboesophageal ganglion. Scale bars = 50μm and 5μm (zoom).

(E) Quantification of PTS1-YFP and PMP70 Pearson colocalization across different cellular populations. $n \geq 3$ brains per genotype, data points represent biological replicates averaged over ≥ 3 ROIs.

(F) Quantification of the number of PTS1-YFP punctate across different cellular populations. $n \geq 3$ brains per genotype, dots represent biological replicates averaged over ≥ 3 ROIs.

* $p < 0.05$, ** $p < 0.01$, *** $p < 0.001$, **** $p < 0.0001$ by Tukey multiple comparisons test.

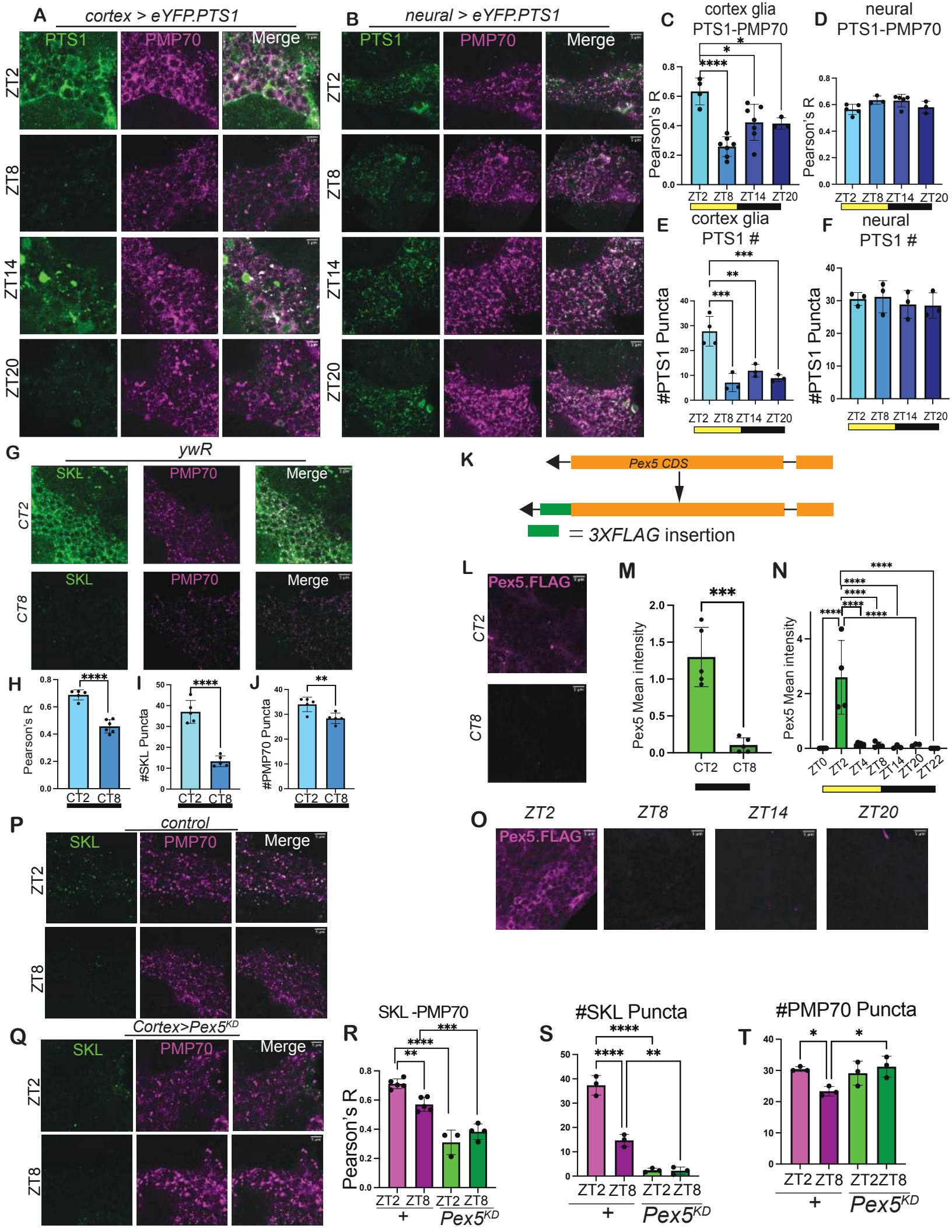
A
cortex > eYFP.PTS1
PTS1
PMP70
Merge
ZT2
ZT8
ZT14
ZT20
B
neural > eYFP.PTS1
C
cortex glia
PTS1-PMP70
Pearson's R
D
neural
PTS1-PMP70
E
cortex glia
PTS1 #
#PTS1 Puncta
F
neural
PTS1 #
G
ywR
SKL
CT2
CT8
H
Pearson's R
I
#SKL Puncta
J
#PMP70 Puncta
K
Pex5 CDS
= 3XFLAG insertion
L
Pex5.FLAG
M
Pex5 Mean intensity
N
O
P
control
Q
Cortex>Pex5KD
R
SKL -PMP70
S
#SKL Puncta
T
#PMP70 Puncta
+
Pex5KD

Figure 2. Peroxisomal import oscillates in cortex glia across time and requires Pex5

(A) Adult female *Drosophila* brains (7 days old) tracking peroxisomal import oscillation across ZT2, ZT8, ZT14, and ZT20 in cortex glia with *UAS-eYFP.PTS1* crossed to *GMR54H02-GAL4*. eYFP-tagged *PTS1*-protein import (green) is counterstained with PMP70 (magenta), an abundant peroxisomal membrane protein. Scale bars = 5μm.

(B) Adult female *Drosophila* brains (7 days old) tracking peroxisomal import oscillation across ZT2, ZT8, ZT14, and ZT20 in neurons with *UAS-eYFP.PTS1* crossed to the pan-neural driver *nSyb-GAL4.* eYFP-tagged *PTS1*-protein import (green) is counterstained with PMP70 (magenta), an abundant peroxisomal membrane protein. Scale bars = 5μm.

(C) Quantification of PTS1-YFP and PMP70 Pearson colocalization across cortex glia. $n \geq 3$ brains per genotype, dots represent biological replicates. ROIs were taken from zooms into cortex below the antennal lobes and above the suboesophageal ganglion.

(D) Quantification of PTS1-YFP and PMP70 Pearson colocalization across neurons. $n \geq 3$ brains per genotype, dots represent biological replicates.

(E) Quantification of the number of PTS1-YFP punctate across cortex glia. $n \geq 3$ brains per genotype, dots represent biological replicates averaged over ≥ 3 ROIs.

(F) Quantification of the number of PTS1-YFP punctate across neurons. $n \geq 3$ brains per genotype, dots represent biological replicates averaged over ≥ 3 ROIs.

(G) Adult female *Drosophila* brains (7 days old) yw^R tracking peroxisomal import oscillation across constant darkness comparing CT2 versus CT8 stained with SKL (green) and PMP70 (magenta), an abundant peroxisomal membrane protein. Scale bars = 5μm.

(H) Quantification of SKL and PMP70 Pearson colocalization. $n \geq 3$ brains per genotype, data points represent biological replicates. ROIs were taken from zooms into cortex below the antennal lobes and above the suboesophageal ganglion.

(I) Quantification of the number of SKL punctate. $n \geq 3$ brains per genotype, dots represent biological replicates averaged over ≥ 3 ROIs.

(J) Quantification of the number of PMP70 punctate. $n \geq 3$ brains per genotype, dots represent biological replicates averaged over ≥ 3 ROIs.

(K) Schema of *Pex5.FLAG* knock-in generated using CRISPR/Cas9-mediated gene editing in *Drosophila*.

(L) Adult female *Drosophila* brains (7 days old) tracking *Pex5.FLAG* knock-in stained with *anti-FLAG* (magenta) across CT2, CT8 (CT = circadian time; animals were entrained on light-dark cycles and then kept in constant darkness for one day)

(M) Quantification of Pex5 mean intensity in constant darkness. *n* ≥*3* brains per genotype, dots represent biological replicates.

(N) Quantification of Pex5 mean intensity in 12hr light/dark cycle. *n* ≥*3* brains per genotype, dots represent biological replicates.

(O) Adult female *Drosophila* brains (7 days old) tracking *Pex5.FLAG* knock-in stained with *anti-FLAG* (magenta) across ZT2, ZT8, ZT14, and ZT20.

(P) Adult female *Drosophila* brains (7 days old) stained with SKL (green) and PMP70 (magenta) in control w^{1118}*/UAS-Pex5 RNAi.*

(Q) Adult female *Drosophila* brains (7 days old) stained with SKL (green) and PMP70 (magenta) in cortex-glia specific knockdown of Pex5 using *GMR54H02-Gal4> UAS-Pex5 RNAi.* ROIs were taken from zooms into cortex below the antennal lobes and above the suboesophageal ganglion.

(R) Quantification of SKL and PMP70 Pearson colocalization. *n* ≥*3* brains per genotype, data points represent biological replicates.

(S) Quantification of the number of SKL punctate. *n* ≥*3* brains per genotype, dots represent biological replicates averaged over ≥*3* ROIs.

(T) Quantification of the number of PMP70 punctate. *n* ≥*3* brains per genotype, dots represent biological replicates averaged over ≥*3* ROIs.

* $p < 0.05$, ** $p < 0.01$, *** $p < 0.001$, **** $p < 0.0001$ by Tukey's multiple comparisons test.

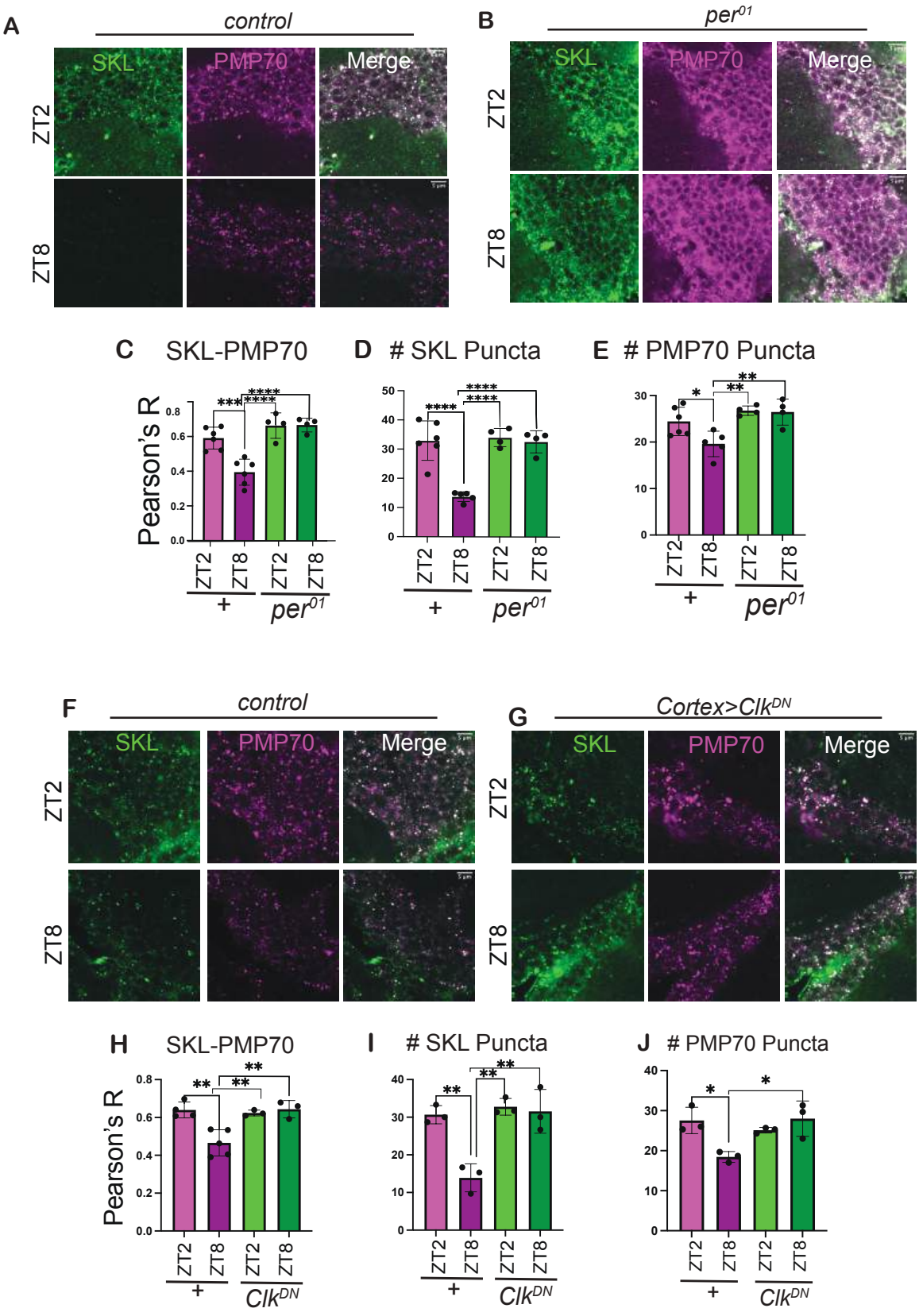
A
control
SKL
PMP70
Merge
ZT2
ZT8
B
per01
SKL
PMP70
Merge
ZT2
ZT8
C SKL-PMP70
Pearson's R
0.0
0.2
0.4
0.6
0.8
***
****
****
ZT2
ZT8
ZT2
ZT8
+
per01
D # SKL Puncta
0
10
20
30
40
50
****
****
****
ZT2
ZT8
ZT2
ZT8
+
per01
E # PMP70 Puncta
0
10
20
30
*
**
**
ZT2
ZT8
ZT2
ZT8
+
per01
F
control
SKL
PMP70
Merge
ZT2
ZT8
G
Cortex>ClkDN
SKL
PMP70
Merge
ZT2
ZT8
H SKL-PMP70
Pearson's R
0.0
0.2
0.4
0.6
0.8
**
**
**
ZT2
ZT8
ZT2
ZT8
+
ClkDN
I # SKL Puncta
0
10
20
30
40
**
**
**
ZT2
ZT8
ZT2
ZT8
+
ClkDN
J # PMP70 Puncta
0
10
20
30
40
*
*
ZT2
ZT8
ZT2
ZT8
+
ClkDN

Figure 3. The circadian clock autonomously controls peroxisomal import in cortex glia

(A) Adult female *Drosophila* brains (7 days old) tracking peroxisomal import oscillation across ZT2, ZT8 in Control (*CantonS*) with SKL (green) counterstained with PMP70 (magenta).

(B) Adult female *Drosophila* brains (7 days old) tracking peroxisomal import oscillation across ZT2, ZT8 in the clock mutant Per^{01} with SKL (green) counterstained with PMP70 (magenta).

(C) Quantification of SKL and PMP70 Pearson colocalization. *n* ≥*3* brains per genotype, data points represent biological replicates averaged over ≥*3* ROIs. ROIs were taken from zooms into cortex below the antennal lobes and above the suboesophageal ganglion.

(D) Quantification of the number of SKL punctate. *n* ≥*3* brains per genotype, dots represent biological replicates averaged over ≥*3* ROIs.

(E) Quantification of the number of PMP70 punctate. *n* ≥*3* brains per genotype, dots represent biological replicates averaged over ≥*3* ROIs.

(F*)* Adult female *Drosophila* brains (7 days old) stained with SKL (green) and PMP70 (magenta) in UAS-control (w^{1118}*/UAS-CLK-DN*)

(G) Adult female *Drosophila* brains (7 days old) stained with SKL (green) and PMP70 (magenta) in Cortex-Glia>*UAS-Clk-Dominant negative(DN) – GMR54H04-Gal4>UAS-CLK-DN.*

(H) Quantification of SKL and PMP70 Pearson colocalization. *n* ≥*3* brains per genotype, data points represent biological replicates averaged over ≥*3* ROIs. ROIs were taken from zooms into cortex below the antennal lobes and above the suboesophageal ganglion.

(I) Quantification of the number of SKL punctate. *n* ≥*3* brains per genotype, dots represent biological replicates averaged over ≥*3* ROIs.

(J) Quantification of the number of PMP70 punctate. *n* ≥*3* brains per genotype, dots represent biological replicates averaged over ≥*3* ROIs.

ns – non-significant, * $p < 0.05$, ** $p < 0.01$, *** $p < 0.001$, **** $p < 0.0001$ by Tukey's multiple comparisons test.

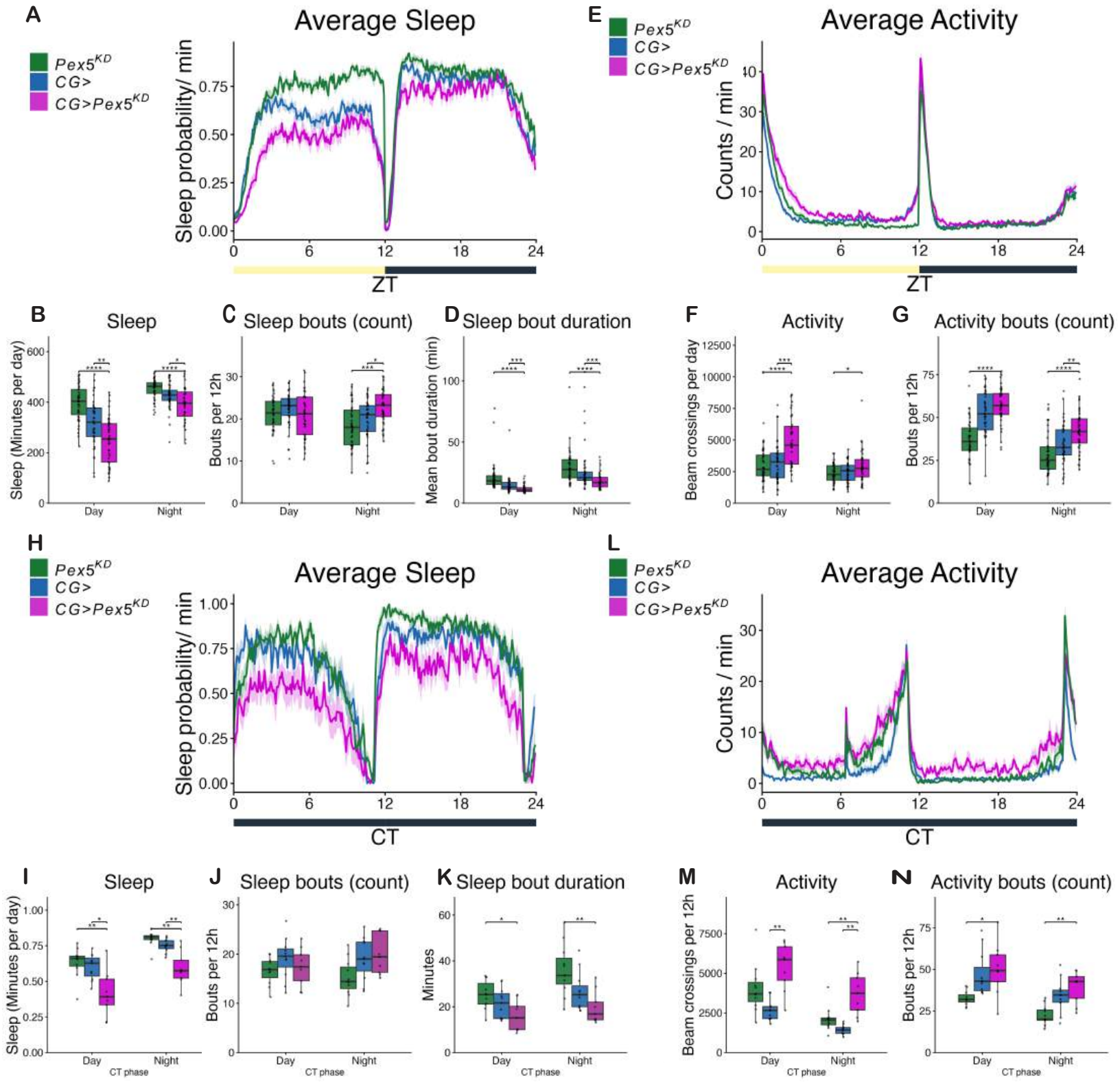
A
Average Sleep
Pex5KD
CG>
CG>Pex5KD
Sleep probability/ min
ZT
E
Average Activity
Counts / min
B
Sleep
Sleep (Minutes per day)
C
Sleep bouts (count)
Bouts per 12h
D
Sleep bout duration
Mean bout duration (min)
F
Activity
Beam crossings per day
G
Activity bouts (count)
Day
Night
H
Average Sleep
CT
L
Average Activity
I
Sleep
J
Sleep bouts (count)
K
Sleep bout duration
Minutes
M
Activity
Beam crossings per 12h
N
Activity bouts (count)
CT phase

Figure 4. Loss of *Pex5* selectively in cortex glia disrupts sleep

(A) Average Sleep (sleep probability/min) was measured for 12hr/12hr, light/dark cycle on an average for 4-5 days continuously for 5-day to 10-day old males post-eclosion. Average sleep time-plot showing sleep probability/min (bouts of inactivity > 5 mins) for the cortex glia driver *GMR77A03-GAL4* crossed with *UAS-Pex5 RNAi-KD* (magenta) compared to parental controls *UAS-Pex5-RNAi (*green) *& GMR77A03-GAL4 (blue)*.

(B) Total sleep(minutes per day) quantified for all three genotypes from **(A).** Individual black dots represent different biological replicates.

(C) Sleep bouts per 12hour quantified for all three genotypes from **(A).** Individual black dots represent different biological replicates.

(D) Sleep bout duration per minute quantified for all three genotypes from **(A).** Individual black dots represent different biological replicates.

(E) Average activity was measured for 12hr/12hr, light/dark cycle on an average for 4-5 days continuously for 5-day to 10-day old males post-eclosion. Average activity time-plot showing counts/min (bouts of inactivity > 5 mins) for the cortex glia driver *GMR77A03- GAL4* crossed with *UAS-Pex5 RNAi KD* (magenta) compared to parental controls *UAS- Pex5-RNAi (*green) *& GMR77A03-GAL4 (blue)*.

(F) Total activity (beam crossings per day) quantified for all three genotypes from **(E).** Individual black dots represent different biological replicates.

(G) Activity bouts (per 12 hour) quantified for all three genotypes from **(E).** Individual black dots represent different biological replicates.

(H) Average Sleep (sleep probability/min) was measured for 12hr/12hr, dark/dark cycle on an average for 5-6 days continuously for 5-day to 10-day old males post-eclosion after initial entrainment on light/dark cycle. Average sleep time-plot showing sleep probability/min (bouts of inactivity > 5 mins) for the cortex glia driver *GMR77A03-GAL4* crossed with *UAS-Pex5 RNAi KD* (magenta) compared to parental controls *UAS-Pex5-RNAi (*green) *& GMR77A03-GAL4 (blue)*.

(I) Total sleep(minutes per day) quantified for all three genotypes from **(H).** Individual black dots represent different biological replicates.

(J) Sleep bouts per 12hour quantified for all three genotypes from **(H).** Individual black dots represent different biological replicates.

(K) Sleep bout duration per minute quantified for all three genotypes from **(H).** Individual black dots represent different biological replicates.

(L) Average activity was measured for 12hr/12hr, dark/dark cycle on an average for 5-6 days continuously for 5-day to 10-day old males post-eclosion after initial entrainment on light/dark cycle. Average activity time-plot showing counts/min (bouts of inactivity > 5 mins) for the cortex glia driver *GMR77A03-GAL4* crossed with *UAS-Pex5 RNAi KD* (magenta) compared to parental controls *UAS-Pex5-RNAi (*green) & *GMR77A03-GAL4 (blue)*.

(M) Total activity (beam crossings per day) quantified for all three genotypes from **(L).** Individual black dots represent different biological replicates.

(N) Activity bouts (per 12 hour) quantified for all three genotypes from **(L).** Individual black dots represent different biological replicates.

* $p < 0.05$, ** $p < 0.01$, *** $p < 0.001$, **** $p < 0.0001$ by ANOVA, Tukey's multiple comparisons or Welch's ANOVA depending on equality of data variance. For nonparametric sleep bouts, Mann-Whitney U test was used. $n \geq 40$ flies for light/dark experiment (Figure 5A-E); $n \geq 10$ flies for dark/dark experiment (Figure 5H-N);

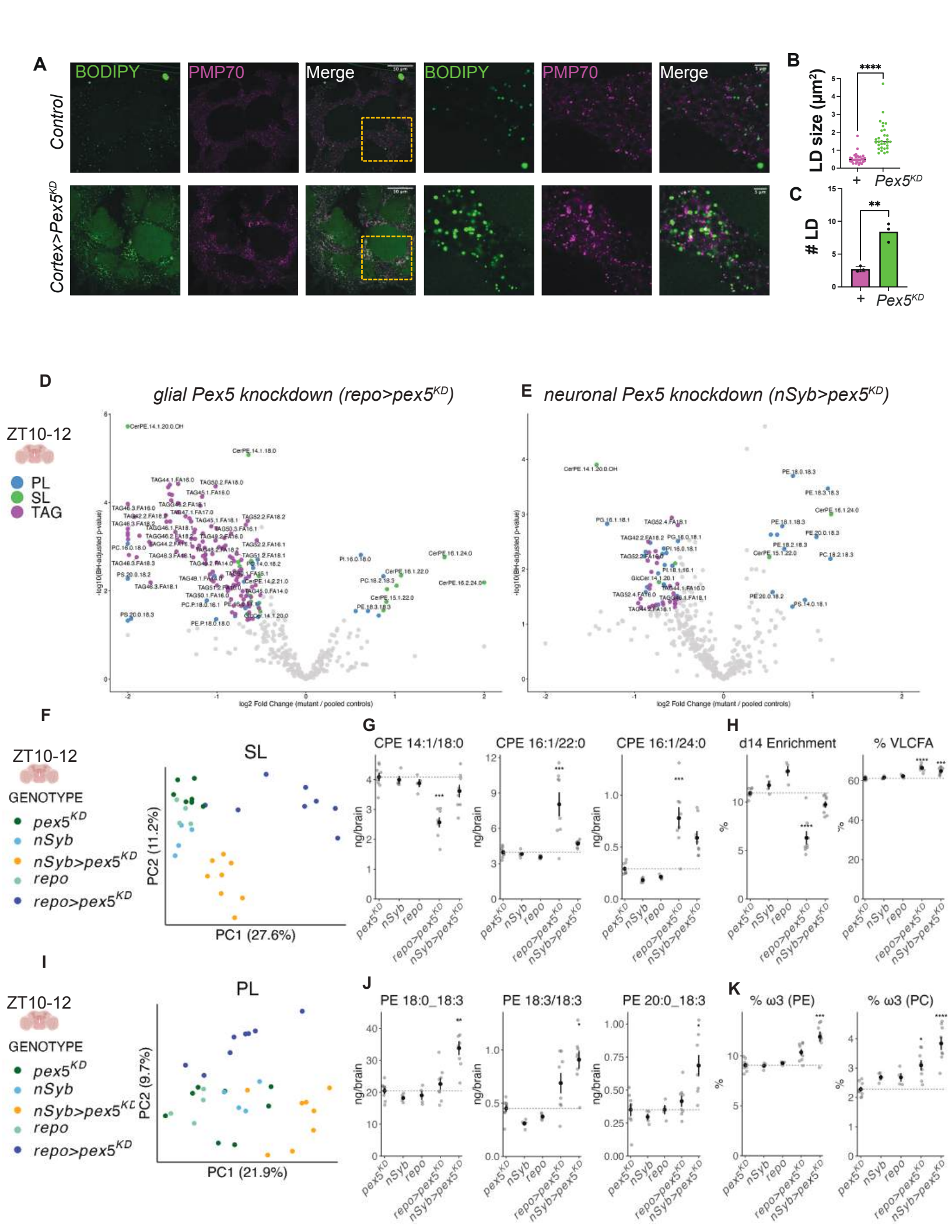
A
BODIPY
PMP70
Merge
Control
Cortex>Pex5KD
B
LD size (μm²)
****
+
Pex5KD
C
LD
**
D
glial Pex5 knockdown (repo>pex5KD)
ZT10-12
PL
SL
TAG
-log10(BH-adjusted p-value)
log2 Fold Change (mutant / pooled controls)
E
neuronal Pex5 knockdown (nSyb>pex5KD)
F
SL
GENOTYPE
pex5KD
nSyb
nSyb>pex5KD
repo
repo>pex5KD
PC2 (11.2%)
PC1 (27.6%)
G
CPE 14:1/18:0
CPE 16:1/22:0
CPE 16:1/24:0
ng/brain
H
d14 Enrichment
% VLCFA
%
I
PL
PC2 (9.7%)
PC1 (21.9%)
J
PE 18:0_18:3
PE 18:3/18:3
PE 20:0_18:3
K
% ω3 (PE)
% ω3 (PC)

Figure 5. Pex5 is essential for lipid homeostasis in the adult brain

A) Adult female *Drosophila* brains (7 days old) tracking neutral lipid droplet (BODIPY 493/503, green) counterstained with PMP70 (magenta). Representative images of UAS-control (*UAS-Pex5 RNAi>w*^{1118}) versus cortex-glia specific knockdown of Pex5 using *GMR54H02-Gal4>UAS-Pex5 RNAi*.

(B) Quantification of different lipid droplet size(um^2) from A.
n ≥*3* brains per genotype, dots represent individual lipid droplets per biological replicates averaged over ≥*3* ROIs. ROIs were taken from zooms into cortex below the antennal lobes and above the suboesophageal ganglion, and quantified from 200x200 pixel windows inside these zooms.

(C) Quantification of lipid droplet count from A. *n* ≥*3* brains per genotype, dots represent number of lipid droplets per biological replicates averaged over ≥*3* ROIs. ROIs were taken from zooms into cortex below the antennal lobes and above the suboesophageal ganglion, and quantified from 200x200 pixel windows inside these zooms.

(D) LC-MS/MS analysis of day 7 female brains at ZT10-12 for glial *Pex5* knockdown; see Table S1 for full genotypic details. Volcano plot shows p-value versus log2foldchange for panglial *pex5*^{KD} versus pooled parental controls. Phospholipids are colored blue, sphingolipids colored green, and TAG colored purple. *n* ≥*4* tubes of 20 brains for each genotype.

(E) LC-MS/MS analysis of day 7 female brains at ZT10-12 for neuronal *Pex5* knockdown. Volcano plot shows p-value versus log2foldchange for pan-neuronal *pex5*^{KD} versus pooled parental controls. Phospholipids are colored blue, sphingolipids colored green, and TAG colored purple. **(F)** Principal component analysis of sphingolipids separates glial *pex5* (blue) and neuronal *pex5* knockdowns (orange) from controls.

(F) Principle component analysis of sphingolipids across the indicated genotypes (orange = neuronal *pex5*^{KD} , dark blue = glial *pex5*^{KD} , light blue = neuronal *GAL4* control, light green = glial *GAL4* control, dark green = *pex5*^{KD} control)

(G) Total ng/brain for select ceramide phosphoethanolamine (CPE) sphingolipids.

(H) Sphingolipid metadata analysis, showing the ratio of d14 sphingolipids over total sphingolipids, and the % of very long chain fatty acids (VLCFA; C > 20).

(I) Principal component analysis of phospholipids separates neuronal *pex5* knockdowns from controls. (orange = neuronal *pex5*^{KD} , dark blue = glial *pex5*^{KD} , light blue = neuronal *GAL4* control, light green = glial *GAL4* control, dark green = *pex5*^{KD} control)

(J) Example ng/brain values for 18:3(omega-3) fatty acid chain containing species that increase upon neuronal *pex5*^{KD}. ω3 fatty acids harbor more than one carbon-carbon double bond, starting from the 3rd carbon away from the terminal of the fatty acid tail.

(K) % of ω3 lipids in phosphatidylethanolamine (PE) and phosphatidylcholine (PC).
* $p < 0.05$, ** $p < 0.01$, *** $p < 0.001$, **** $p < 0.0001$ by Tukey's multiple comparisons test.

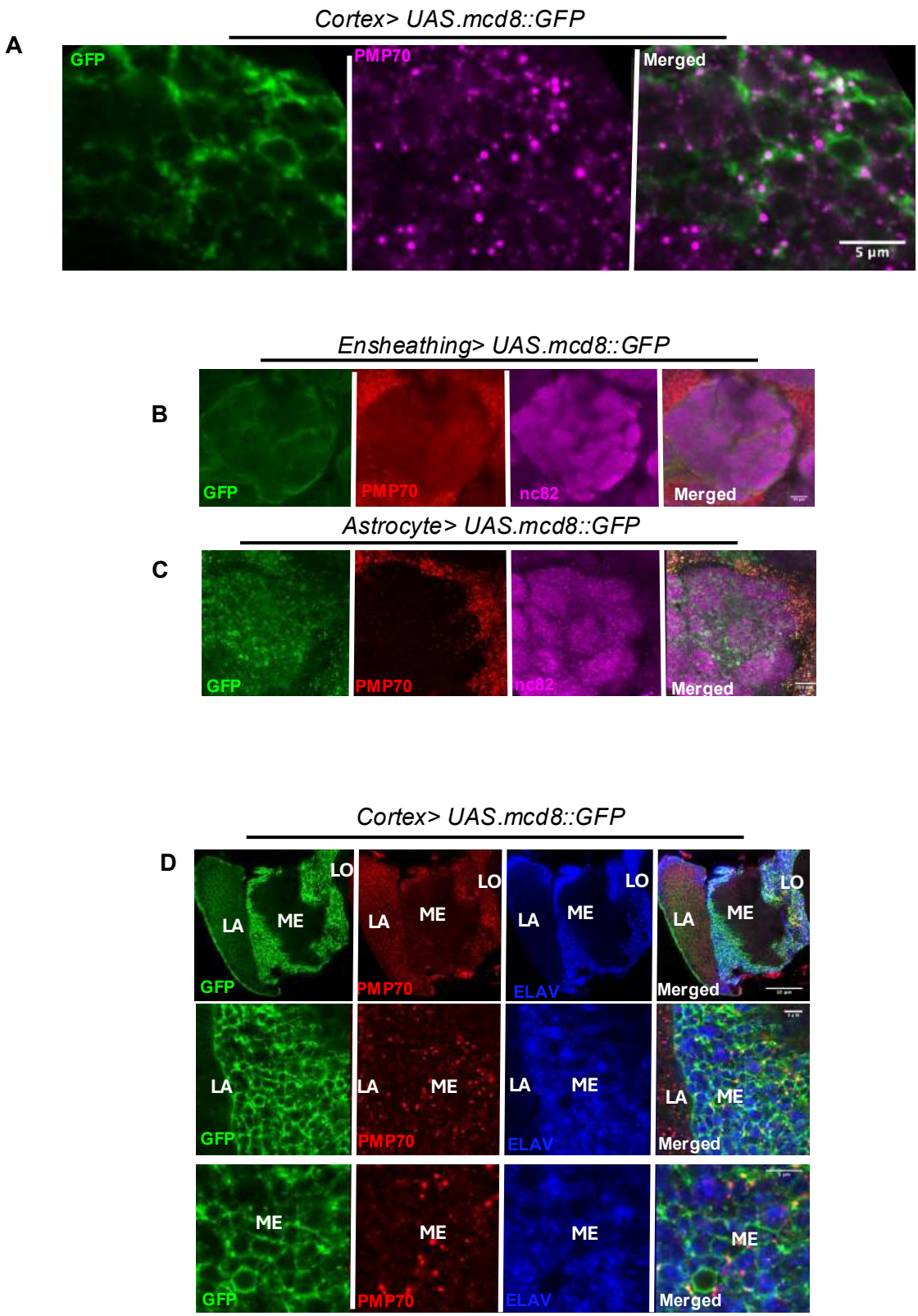

Figure 1 Supplemental - related to figure 1

Figure S1, related to Figure1

Representative images comparing central brain glial classes, with colocalization between glial driven GFP(green) counterstained with PMP70(magenta). PMP70 peroxisomes are abundant inside cortex glial regions as compared to astrocyte and ensheathing glia. nC82(magenta) marks the pre-synaptic active zones representing the neuropils of the adult *Drosophila* brain.

(A) Adult female *Drosophila* brains (7 days old) Cortex glia (*GMR54H02*-GAL4> UAS-*mCD8::GFP*) tracking colocalization between GFP(green) counterstained with PMP70(magenta).

(B) Adult female *Drosophila* brains (7 days old) Ensheathing glia (*GMR56F03-GAL4>* UAS-*mCD8::GFP*) tracking colocalization between GFP(green) counterstained with PMP70(red) and nc82 (magenta).

(C) Adult female *Drosophila* brains (7 days old) astrocytic glia (*alrm-GAL4> UAS-mCD8::GFP*) tracking colocalization between GFP(green) counterstained with PMP70(red) and nc82 (magenta).

D) Adult female *Drosophila* brains (7 days old) Cortex glia (*GMR54H02*-GAL4> UAS-*mCD8::GFP*) representative image showing the optic lobe regions (LA-lamina; ME-medulla; LO-lobula) showing PMP70 (red) positive puncta in GFP(green) rich regions of cortex.

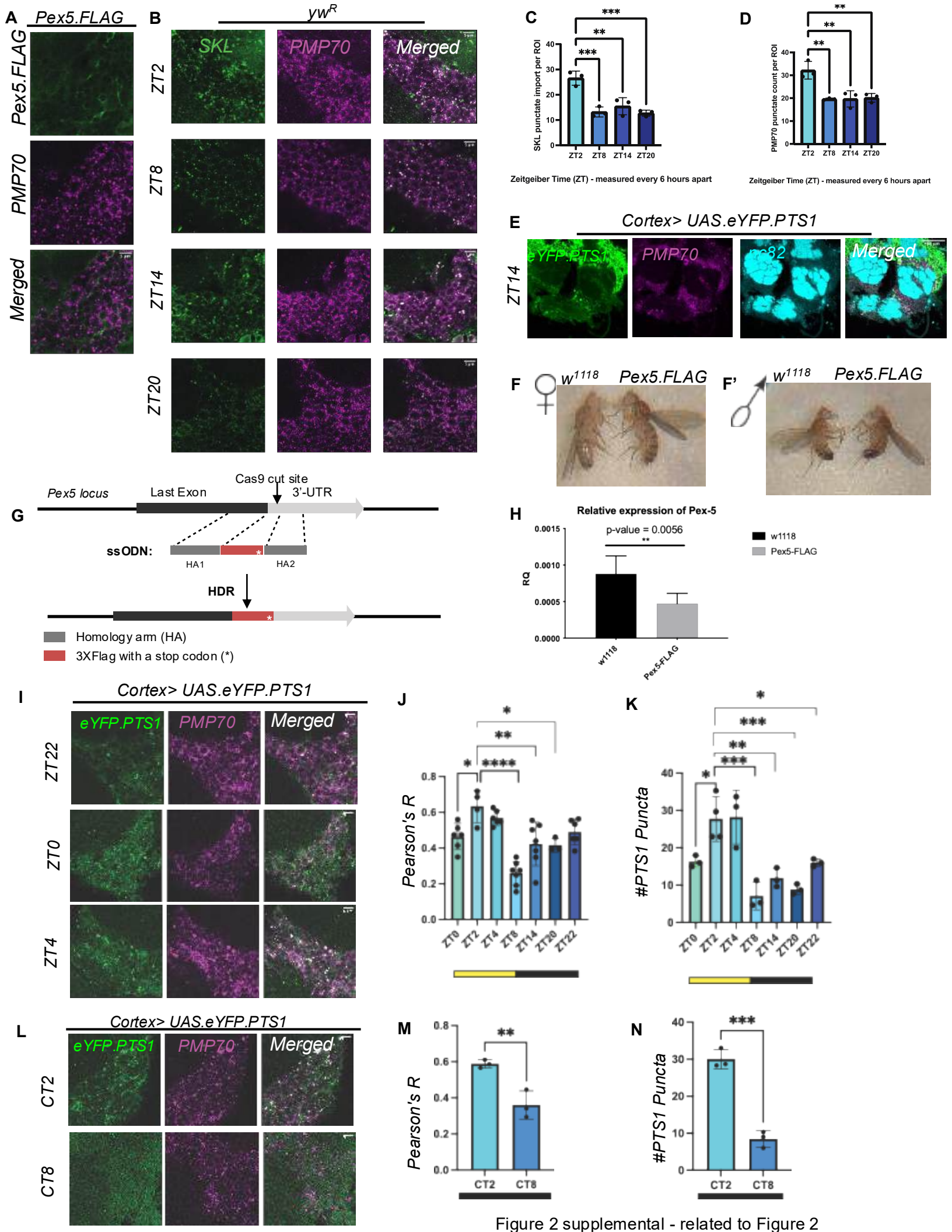

Figure 2 supplemental - related to Figure 2

Figure S2, related to Figure 2.
(A) Adult female *Drosophila* brains (7 days old) tracking Pex5.FLAG knock-in flies co-stained with anti-FLAG(green) and anti-PMP70(magenta).

(B)Adult female *Drosophila* brains (7 days old) yw^R wildtype flies dissected across ZT2, ZT8, ZT14 and ZT20 and stained with anti-SKL(green), anti-PMP70(magenta) to show circadian oscillations of peroxisomal import peak at ZT2 and trough at ZT8.

(C) Quantification in yw^R wildtype flies of *SKL* puncta at ZT2, ZT8, ZT14, ZT20. $n \geq 3$ brains per genotype, dots represent biological replicates averaged over ≥ 3 ROIs. ROIs were taken from zooms into cortex below the antennal lobes and above the suboesophageal ganglion.

(D) Quantification in yw^R wildtype flies of PMP70 puncta at ZT2, ZT8, ZT14, ZT20; $n \geq 3$ brains per genotype, dots represent biological replicates averaged over ≥ 3 ROIs.

(E) Adult female *Drosophila* brains (7 days old) tracking peroxisomal import oscillation at ZT14 observed in glia with *UAS-eYFP.PTS1* using *GMR54H02-GAL4*. eYFP-tagged *PTS1*-protein import (green) is counterstained with PMP70 (magenta), an abundant peroxisomal membrane protein to detect peroxisomes along with anti-nc82. Scale bar = 50µm.

(F) Adult female *Drosophila* comparing w^{1118} versus *Pex5.FLAG.*

(F') Adult male *Drosophila* comparing w^{1118} versus *Pex5.FLAG.*

(G) CRISPR/Cas9-based knock-in strategy to tag *Pex5* with a 3XFLAG epitope.

(H) Relative transcript expression of Pex5 in w1118 versus Pex5.FLAG measured by RT-qPCR (full flies, adult female; 7 days old) at ZT2.

(I) Adult female *Drosophila* brains (7 days old) *Cortex>UAS-eYFP.PTS1* flies dissected across ZT22, ZT0 and ZT4 stained with anti-GFP(green), anti-PMP70(magenta).

(J) Quantification of eYFP-PTS1 and PMP70 Pearson colocalization. $n \geq 3$ brains per genotype, data points represent biological replicates.

(K) Quantification of the number of PTS1 punctate. $n \geq 3$ brains per genotype, dots represent biological replicates averaged over ≥ 3 ROIs.

(L) Adult female *Drosophila* brains (7 days old) *Cortex>UAS-eYFP.PTS1* flies dissected across CT2 and CT8 (CT = circadian time) in 12hr/2hr dark/dark cycle after initial light/dark entrainment stained with anti-GFP(green), anti-PMP70(magenta).

(M) Quantification of eYFP-PTS1 and PMP70 Pearson colocalization. $n \geq 3$ brains per genotype, data points represent biological replicates.

(N) Quantification of the number of PTS1 punctate. *n* ≥*3* brains per genotype, dots represent biological replicates averaged over ≥*3* ROIs. ROIs were taken from zooms into cortex below the antennal lobes and above the suboesophageal ganglion.

* $p < 0.05$, ** $p < 0.01$, *** $p < 0.001$, **** $p < 0.0001$ by Tukey's multiple comparisons test.

A

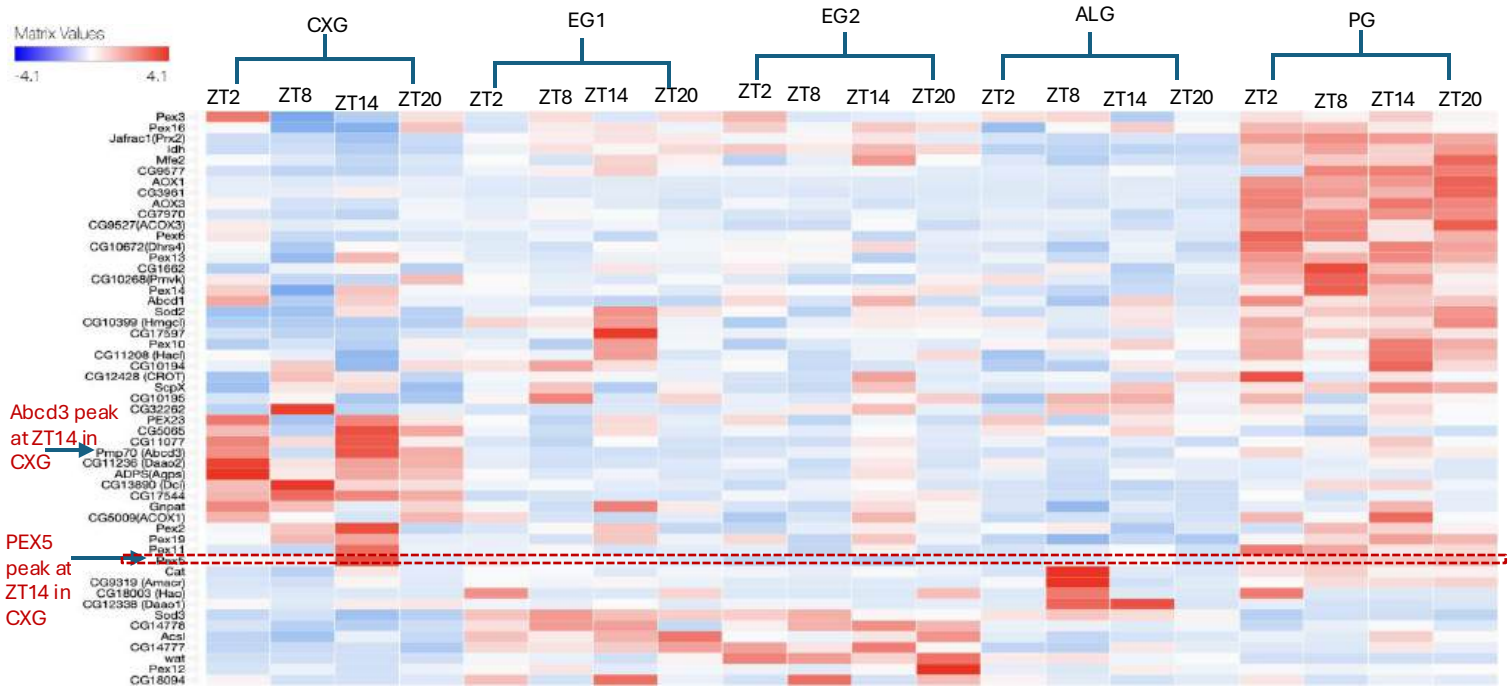

Global Heat map of peroxisomal differentially expressed genes in glial clusters at different ZT (zeitgeber) time points from Drosophila sleep single-cell

B

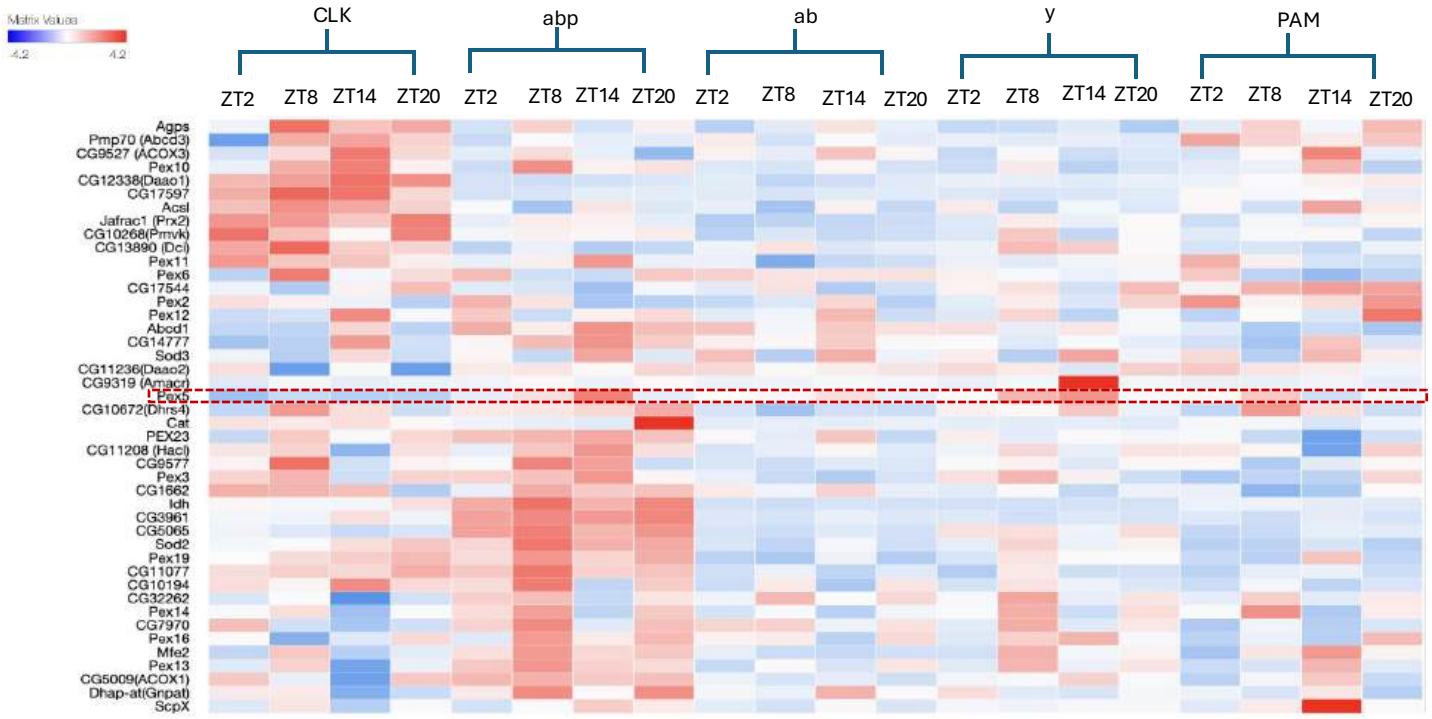

Global Heat map of peroxisomal differentially expressed genes in Neuronal clusters from Drosophila sleep single-cell

Figure 3- Supplemental

Figure S3, related to Figure 2.
(A) Global heatmap of peroxisomal gene expression extracted from fly-sleep single across all glial clusters to show *Pex5* expression is highest in CXG *(*cortex-glia) cluster.

(B) Global heatmap of peroxisomal gene expression extracted from fly-sleep single across neuronal clusters to show low *Pex5* expression as opposed to CXG glial cluster.

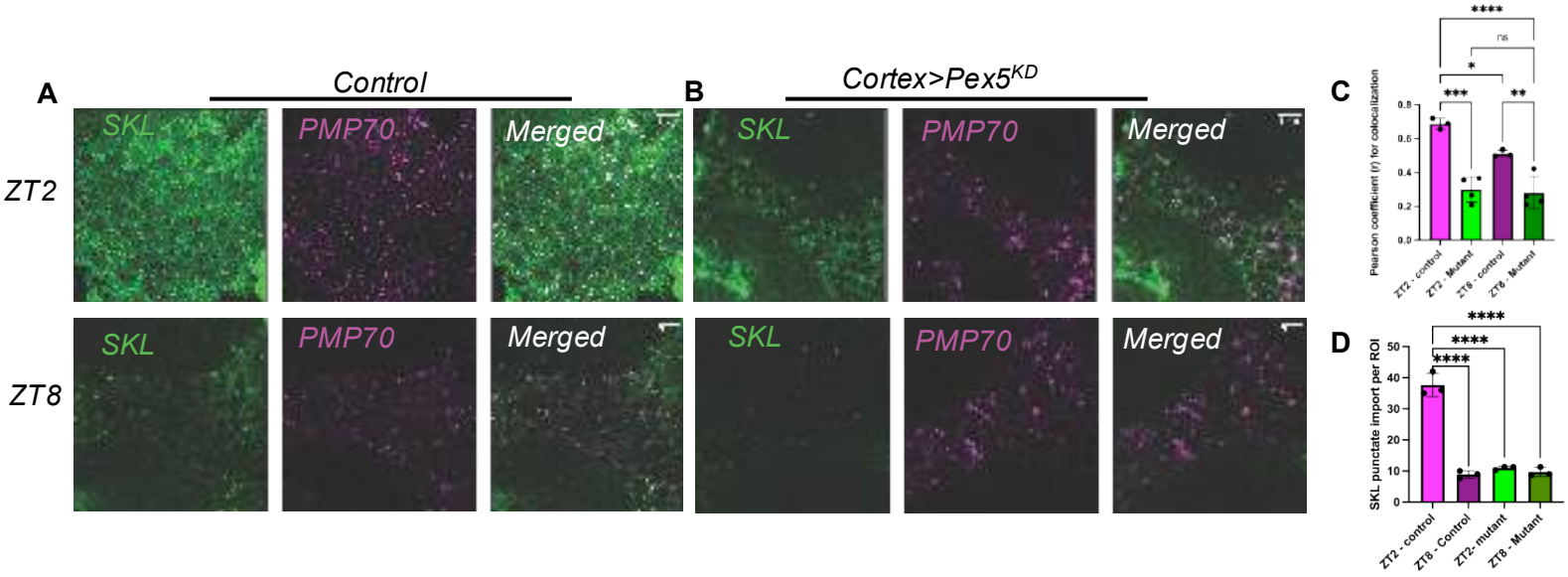

Figure 4 Supplemental - related to figure 2

Figure S4, related to Figure 2.

(A) Adult female *Drosophila* brains (7 days old) Control (w^{1118} */UAS-Pex5* RNAi) flies dissected across ZT2 and ZT8 stained with anti-SKL(green), anti-PMP70(magenta) to show circadian oscillations of peroxisomal import peak at ZT2 and trough at ZT8.

(B) Adult female *Drosophila* brains (7 days old) mutants (*Cortex* > *UAS-Pex5 RNAi;* (BDSC# 55322) flies dissected across ZT2 and ZT8 stained with anti-SKL(green), anti-PMP70(magenta).

(C) Quantification of SKL and PMP70 Pearson colocalization. $n \geq 3$ brains per genotype, data points represent biological replicates. ROIs were taken from zooms into cortex below the antennal lobes and above the suboesophageal ganglion.

(D) Quantification of the number of SKL punctate. $n \geq 3$ brains per genotype, dots represent biological replicates averaged over ≥ 3 ROIs.

* $p < 0.05$, ** $p < 0.01$, *** $p < 0.001$, **** $p < 0.0001$ by Tukey's multiple comparisons test.

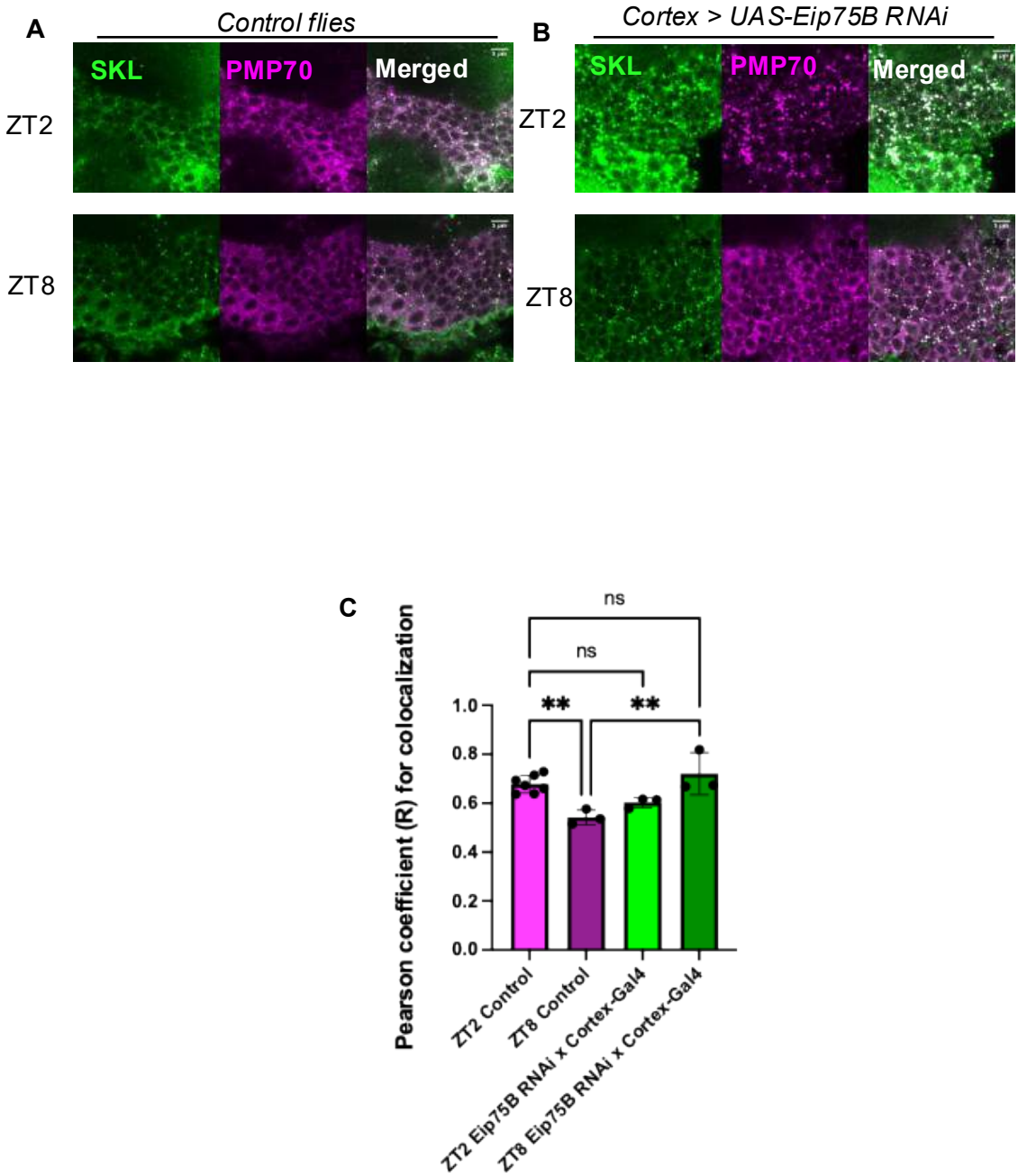

Figure 5 Supplemental - related to Figure 3

Figure S5, related to Figure 3.
(A) Adult female *Drosophila* brains (7 days old) dissected at ZT2 & ZT8 for control flies (w^{1118}/*UAS-Eip75B RNAi*) stained with anti-SKL(green) and anti-PMP70(magenta).

(B) Adult female *Drosophila* brains (7 days old) dissected at ZT2 & ZT8 for *GMR54H02-Gal4>UAS-Eip75B RNAi* knockdown flies.

(C) Quantification Pearson R coefficient colocalization calculated (see methods) for *GMR54H02-Gal4* cross with *UAS-Eip75B* RNAi knockdown flies compared with control flies at ZT2, ZT8; $n \geq 3$ brains per genotype, dots represent biological replicates averaged over ≥ 3 ROIs. ROIs were taken from zooms into cortex below the antennal lobes and above the suboesophageal ganglion,

* $p < 0.05$, ** $p < 0.01$, *** $p < 0.001$, **** $p < 0.0001$ by Tukey's multiple comparisons test.

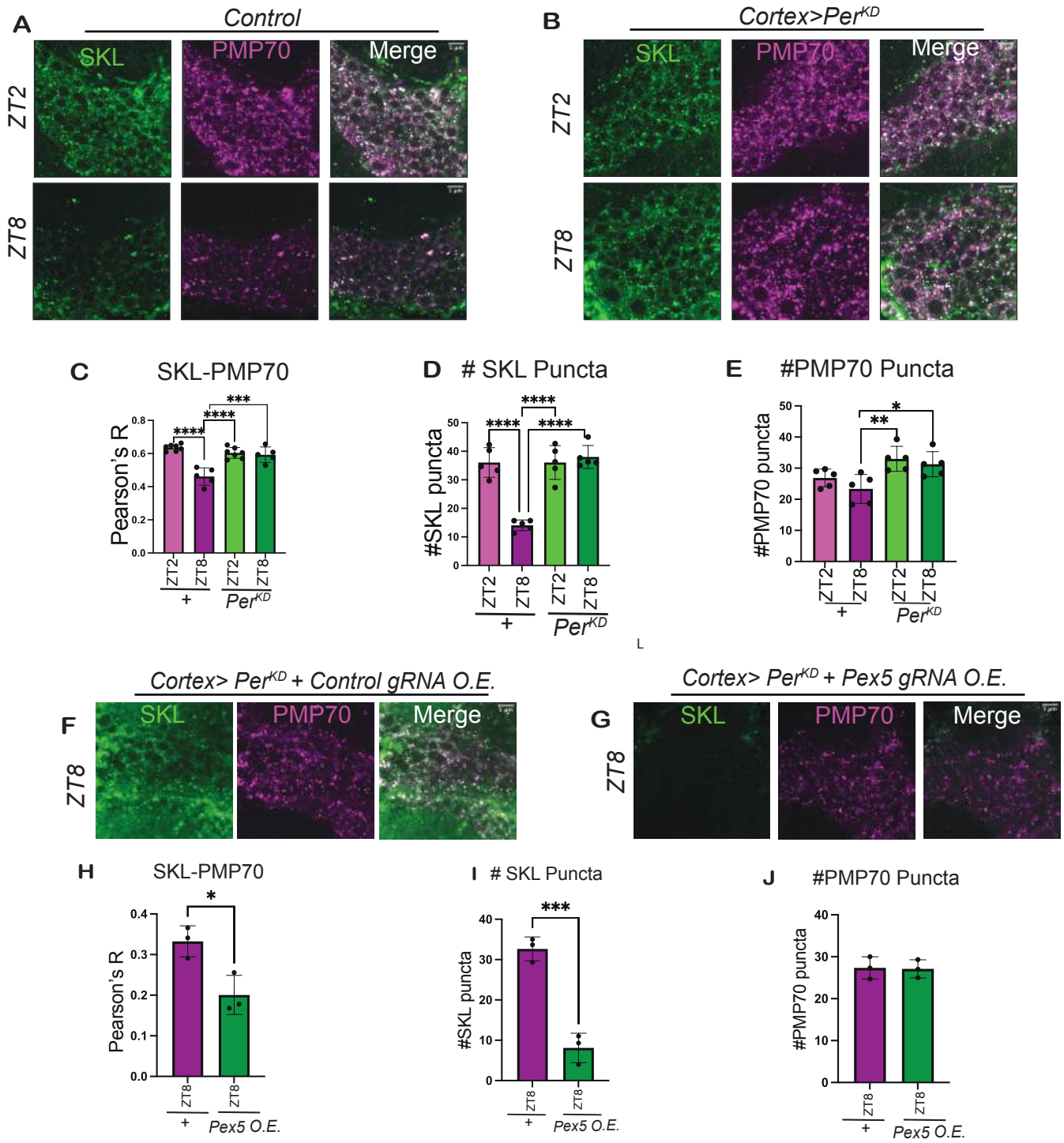

Figure 6 Supplemental - Related to Figure 3

Figure S6, related to Figure 3. Pex5 overexpression in cortex glia rescues Per controlled peroxisomal decline at ZT8

(A) Adult female *Drosophila* brains (7 days old) tracking peroxisomal import oscillation across ZT2, ZT8 in Control *>w1118/GMR54H02-Gal4)* with SKL (green) counterstained with PMP70 (magenta).

(B) Adult female *Drosophila* brains (7 days old) tracking peroxisomal import oscillation across ZT2, ZT8 in *Cortex-Glia> UAS-Per RNAi* (*GMR54H02-Gal4>UAS-Per RNAi)* with SKL (green) counterstained with PMP70 (magenta).

(C) Quantification of SKL and PMP70 Pearson colocalization. *n* ≥*3* brains per genotype, data points represent biological replicates averaged over ≥*3* ROIs. ROIs were taken from zooms into cortex below the antennal lobes and above the suboesophageal ganglion,

(D) Quantification of the number of SKL punctate. *n* ≥*3* brains per genotype, dots represent biological replicates averaged over ≥*3* ROIs.

(E) Quantification of the number of PMP70 punctate. *n* ≥*3* brains per genotype, dots represent biological replicates averaged over ≥*3* ROIs.

(F*)* Adult female *Drosophila* brains (7 days old) stained with SKL (green) and PMP70 (magenta) with cortex glial knockdown of *Per*, combined with UAS-Cas9.VPR expressing non-targeting gRNA control (*w- / y[1]w[1]; UAS-3xFLAG.dCas9.VPR/non-targeting control gRNA; UAS-Per RNAi/GMR54H02-GAL4).*

(G) Adult female *Drosophila* brains (7 days old) stained with SKL (green) and PMP70 (magenta) with cortex glial knockdown of *Per*, with *UAS-Cas9.VPR* overexpressing *Pex5 gRNA* (*w- / y[1]w[1]; UAS-3xFLAG.dCas9.VPR/Pex5 gRNA; UAS-Per RNAi/GMR54H02- Gal4*)

(H) Quantification of SKL and PMP70 Pearson colocalization. *n* ≥*3* brains per genotype, data points represent biological replicates averaged over ≥*3* ROIs. ROIs were taken from zooms into cortex below the antennal lobes and above the suboesophageal ganglion,

(I) Quantification of the number of SKL punctate. *n* ≥*3* brains per genotype, dots represent biological replicates averaged over ≥*3* ROIs.

(J) Quantification of the number of PMP70 punctate. *n* ≥*3* brains per genotype, dots represent biological replicates averaged over ≥*3* ROIs.

* $p < 0.05$, ** $p < 0.01$, *** $p < 0.001$, **** $p < 0.0001$ by Tukey's multiple comparisons test.

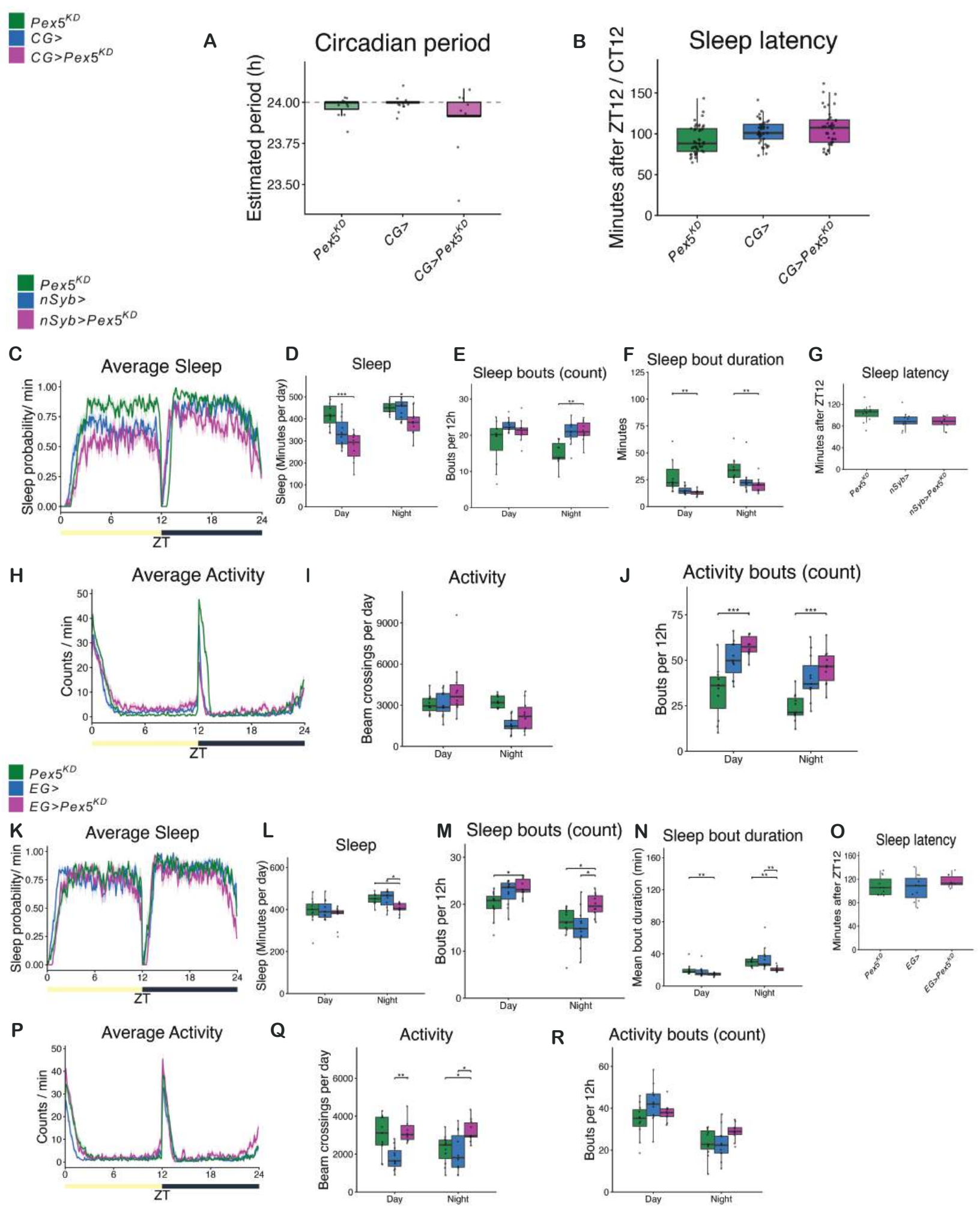

Figure 7 Supplemental - related to Figure 4

Figure S7,related to Figure4. Loss of *Pex5* sleep and activity analyzed for neuronal and ensheathing glia.

(A) Circadian period length measured in 12hr/12hr, dark/dark cycle on an average for 5-6 days continuously for 5-day to 10-day old males post-eclosion after initial entrainment in 12hr/12hr, light/dark for cortex glia driver *GMR77A03-GAL4* crossed with *UAS-Pex5 RNAi KD* (magenta) compared to parental controls *UAS-Pex5-RNAi (*green) *& GMR77A03-GAL4 (blue)*.

(B) Sleep latency was measured after lights off in 12hr/12hr, light/dark cycle on an average for 4-5 days continuously for 5-day to 10-day old males post-eclosion for cortex glia driver *GMR77A03-GAL4* crossed with *UAS-Pex5 RNAi KD* (magenta) compared to parental controls *UAS-Pex5-RNAi (*green) *& GMR77A03-GAL4 (blue)*.

(C) Average Sleep (sleep probability/min) measured in 12hr/12hr, light/dark cycle on an average for 4-5 days continuously for 5-day to 10-day old males post-eclosion. Average sleep time-plot showing sleep probability/min (bouts of inactivity > 5 mins) for the neuronal driver *nSyb-GAL4* crossed with *UAS-Pex5 RNAi KD* (magenta) compared to parental controls *UAS-Pex5-RNAi (*green) *& nSyb-GAL4 (blue)*.

(D) Total sleep(minutes per day) quantified for all three genotypes from **(C).** Individual black dots represent different biological replicates.

(E) Sleep bouts per 12hour quantified for all three genotypes from **(C).** Individual black dots represent different biological replicates.

(F) Sleep bout duration per minute quantified for all three genotypes from **(C).** Individual black dots represent different biological replicates.

(G) Sleep latency quantified for all three genotypes from **(C).** Individual black dots represent different biological replicates.

(H) Average activity measured in 12hr/12hr, light/dark cycle on an average for 4-5 days continuously for 5-day to 10-day old males post-eclosion. Average activity time-plot showing counts/min (bouts of inactivity > 5 mins) for the neuronal driver *nSyb-GAL4* crossed with *UAS-Pex5 RNAi KD* (magenta) compared to parental controls *UAS- Pex5-RNAi (*green) *& nSyb-GAL4 (blue)*.

(I) Total activity (beam crossings per day) quantified for all three genotypes from **(H).** Individual black dots represent different biological replicates.

(J) Activity bouts (per 12 hour) quantified for all three genotypes from **(H).** Individual black dots represent different biological replicates.

(K) Average Sleep (sleep probability/min) measured in 12hr/12hr, dark/dark cycle on an average for 5-6 days continuously for 5-day to 10-day old males post-eclosion after

initial entrainment on light/dark cycle. Average sleep time-plot showing sleep probability/min (bouts of inactivity > 5 mins) for the ensheathing glia driver *GMR56F03-GAL4* crossed with *UAS-Pex5 RNAi KD* (magenta) compared to parental controls *UAS-Pex5- RNAi (*green) *& GMR56F03-GAL4 (blue)*.

(L) Total sleep(minutes per day) quantified for all three genotypes from **(K).** Individual black dots represent different biological replicates.

(M) Sleep bouts per 12hour quantified for all three genotypes from **(K).** Individual black dots represent different biological replicates.

(N) Sleep bout duration per minute quantified for all three genotypes from **(K).** Individual black dots represent different biological replicates.

(O) Sleep latency quantified for all three genotypes from **(K).** Individual black dots represent different biological replicates.

(P) Average activity measured in 12hr/12hr, dark/dark cycle on an average for 5-6 days continuously for 5-day to 10-day old males post-eclosion after initial entrainment on light/dark cycle. Average activity time-plot showing counts/min (bouts of inactivity > 5 mins) for the ensheathing glia driver *GMR56F03-GAL4* crossed with *UAS-Pex5 RNAi KD* (magenta) compared to parental controls *UAS-Pex5-RNAi (*green) *GMR56F03-GAL4 (blue)*.

(Q) Total activity (beam crossings per day) quantified for all three genotypes from **(P).** Individual black dots represent different biological replicates.

(R) Activity bouts (per 12 hour) quantified for all three genotypes from **(P).** Individual black dots represent different biological replicates.

* $p < 0.05$, ** $p < 0.01$, *** $p < 0.001$, **** $p < 0.0001$ by ANOVA, Tukey's multiple comparisons or Welch's ANOVA depending on equality of data variance. For nonparametric sleep bouts, Mann-Whitney U test was used. $n \geq 10$ flies for light/dark experiment.

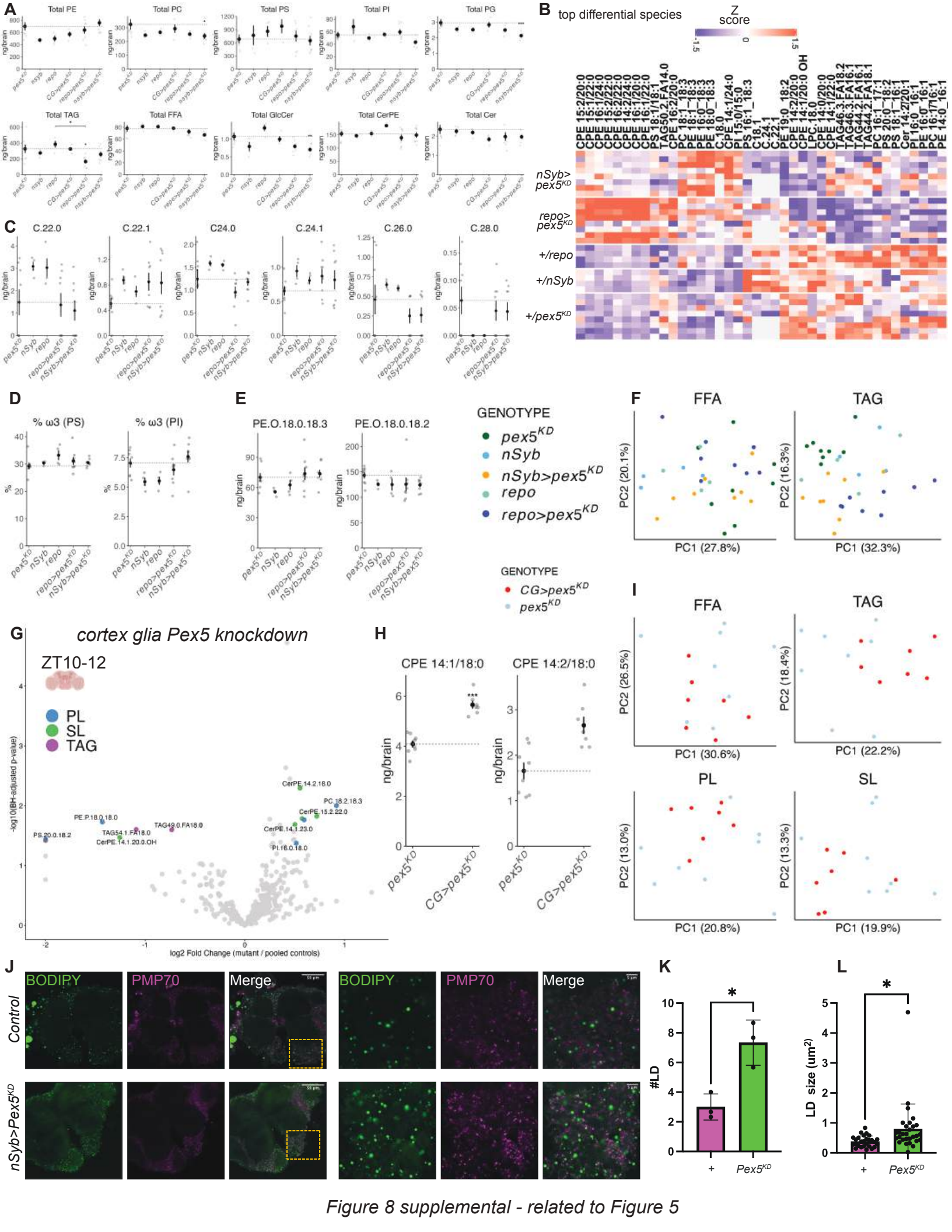

Figure 8 supplemental - related to Figure 5

Figure S8, related to Figure5. Pex5 is essential for lipid homeostasis in the adult brain.

(A) Total ng/brain for lipid families analyzed by LC-MS/MS of day 7 females brains at ZT10-12; see Table S1 for full genotypic details. *n ≥4* tubes of 20 brains for each genotype.

(B) Heatmap of top 30 species changed between controls and mutants, z-scored by relative % abundance.

(C) Free fatty acid analysis of longer chain fatty acid species across genotype, including very long chain fatty acids (VLCFA) (ng/brain)

(D) % of ω3 fatty acids in phosphatidylserine (PS) and phosphatidylinositol (PI).

(E) Major alky-ether phospholipids shown in ng/brain across genotypes.

(F) Principal component analysis of TAGs and free fatty acids (FFA) colored by genotype.

(G) Volcano plot showing p-value versus log2 fold change for cortex glia *pex5* knockdown versus parental controls. Phospholipids are colored green, sphingolipids colored green, and TAG colored purple.

(H) Differentially abundant ceramide phosphoethanolamine (CPE) species in *CG* > $pex5^{KD}$ brains.

(I) principal component analysis of controls versus *CG* > $pex5^{KD}$ brains (red) versus control (grey) for sphingolipids (SL), phospholipids (PL), TAG, and free fatty acids (FFA).

(J) Adult female *Drosophila* brains (7 days old) tracking neutral lipid droplet (BODIPY 493/503, green) counterstained with PMP70 (magenta). Representative images of UAS-control (*UAS-Pex5 RNAi* > w^{1118}) versus neuronal specific knockdown of Pex5 using *nSyb-Gal4* > *UAS-Pex5 RNAi*.

(K) Quantification of different lipid droplet size(um^2) from J.
n ≥3 brains per genotype, dots represent individual lipid droplets per biological replicates averaged over ≥*3* ROIs. ROIs were taken from zooms into cortex below the antennal lobes and above the suboesophageal ganglion, and quantified from 200x200 pixel windows inside these zooms.

(L) Quantification of lipid droplet count from J. *n ≥3* brains per genotype, dots represent number of lipid droplets per biological replicates averaged over ≥*3* ROIs.

* $p < 0.05$, ** $p < 0.01$, *** $p < 0.001$, **** $p < 0.0001$ by Tukey's multiple comparisons test.

RESOURCE AVAILABILITY

Lead contact

Correspondence should be directed to Anurag Das (anuragd7@iastate.edu)

Materials availability

All data and code reported in this paper will be shared by the lead contact (AD) upon request.

Acknowledgements

We thank Bai lab members for feedback during lab meetings. We thank Bloomington Drosophila Stock Center (NIH P40OD018537) for fly stocks. We thank FlyBase (NHGRI U41HG000739) for *Drosophila* gene annotation. We thank Kyu-Sun Lee for fly Pmp70 antibodies. We thank Abhilash Goswami for providing suggestions for the extraction of peroxisomal genes from publicly available single cell data. We thank Elizabeth McNeill, Amita Sehgal, and Marc Tatar for sharing fly stocks. We thank Alicia Taylor from the Elizabeth McNeill Lab for providing DAM5H-Trikinetics Drosophila Sleep Activity Monitoring system for our sleep studies. Graphical model figures were created with BioRender.com. This work was supported by NSF CAREER 2046984, Hevolution HF-GRO-23-1199062-14, and NIH R01AG075156 to HB. JPV is supported by the Sandler PBBR grant and the Simons Foundation.

Author contributions

Conceptualization: Anurag Das, Hua Bai
Methodology: Anurag Das, John Philip Vaughen, Irma Magaly Rivas-Serna, Ankur Kumar, Ruiqi Liu, Kerui Huang, Hua Bai
Formal Analysis: Anurag Das, John Philip Vaughen, Marlene Dorneich-Hayes, Lakpa Sherpa
Investigation: Anurag Das, John Philip Vaughen, Irma Magaly Rivas-Serna, Marlene Dorneich-Hayes, Lakpa Sherpa
Visualization: Anurag Das, John Philip Vaughen, Hua Bai
Funding Acquisition: John Philip Vaughen, Vera Mazurak, Hua Bai
Project Administration: Anurag Das, John Philip Vaughen, Hua Bai
Supervision: John Philip Vaughen, Hua Bai
Writing (original draft): Anurag Das
Writing (review & editing): Anurag Das, John Philip Vaughen
Revisions: Anurag Das, John Philip Vaughen

Declaration of interests

The authors declare no competing interests.

Resources table

REAGENT or RESOURCE	SOURCE	IDENTIFIER
Antibodies		
Fly-PMP70	a gift from Kyu-Sun Lee	N/A
Anti-ELAV	DSHB	Rat-Elav-7E8A10 anti-elav
Anti-nc82	DSHB	nc82
Monoclonal Anti-FLAG	Sigma-Aldrich	F1804
Anti-SKL	a gift from Richard Rachubinski	N/A
Anti-GFP mAb	Cell Signaling Technology	2956
Experimental models: Organisms/strains		
D. melanogaster: *w*^{1118}	BDSC	Cat# 5905; RRID: BDSC_5905
D. melanogaster: *ywR*	A gift from Marc Tatar	N/A
D. melanogaster: *CantonS*	A gift from Elizabeth McNeill	N/A
D. melanogaster: *per[01]*	BDSC	Cat# 80928; RRID: BDSC_80928
D. melanogaster: *w[1118]; P{y[+t7.7] w[+mC]=GMR77A03-GAL4}attP2*	BDSC	Cat# 39944; RRID: BDSC_39944
D. melanogaster: *w[1118]; P{y[+t7.7] w[+mC]=GMR54H02-GAL4}attP2*	BDSC	Cat# 45784; RRID: BDSC_45784
D. melanogaster: *y[1] v[1]; P{y[+t7.7] v[+t1.8]=TRiP.HMJ21920}attP40*	BDSC	Cat# 58064; RRID: BDSC_58064
D. melanogaster: *w[1118]; P{y[+t7.7] w[+mC]=GMR57C10-GAL4}attP2*	BDSC	Cat# 39171; RRID: BDSC_39171
D. melanogaster: *y[1] sc[*] v[1] sev[21]; P{y[+t7.7] v[+t1.8]=TRiP.HMS01530}attP40*	BDSC	Cat# 35780; RRID: BDSC_35780
D. melanogaster: *w[1118]; P{y[+t7.7] w[+mC]=GMR56F03-GAL4}attP2*	BDSC	Cat# 39157; RRID: BDSC_39157
D. melanogaster: *w[1118]; P{y[+t7.7] w[+mC]=GMR83E10-GAL4}attP2*	BDSC	Cat# 40362; RRID: BDSC_40362
D. melanogaster: *Pex5[FLAG-a1]/FM7a*	This paper	N/A
D. melanogaster: *w[1118]; P{w[+m*]=GAL4}repo/TM3, Sb[1]*	BDSC	Cat# 7415; RRID: BDSC_7415
D. melanogaster: *w[*]; P{w[+mC]=UAS-eYFP.PTS1}6*	BDSC	Cat# 64248; RRID: BDSC_64248
D. melanogaster: *y[1] w[*]; betaTub60D[Pin-Yt]/CyO; P{w[+mC]=UAS-mCD8::GFP.L}LL6*	BDSC	Cat# 5130; RRID: BDSC_5130
D. melanogaster: *w[*]; wg[Sp-1]/CyO; P{w[+m*]=alrm-GAL4.D}2*	BDSC	Cat# 67032; RRID: BDSC_67032
D. melanogaster: y[1] v[1]; P{y[+t7.7]=CaryP}Msp300[attP40]	BDSC	Cat# 36304; RRID: BDSC_36304
D. melanogaster: repo-GAL4 =. +; *UAS-Dcr-2* (BDSC 24650)*/+; repo-GAL4* (BDSC 7415)*/+*	This paper	N/A
D. melanogaster: nSyb-GAL4 = +; *UAS-Dcr-2/+; nSyb-GAL4* (BDSC 39171)*/+*	This paper	N/A
D. melanogaster: repo > pex5^{KD} = +; *UAS-Dcr-2/pex5-trip; repo-GAL4/+*	This paper	N/A

*D. melanogaster: CG > pex5^{KD} = +; pex5-trip/+; GMR54H02-GAL4(*BDSC 45784)/+	This paper	N/A
D. melanogaster: nSyb > pex5^{KD} = + ; UAS-Dcr-2/pex5-trip; nSyb-GAL4/+ ;	This paper	N/A
D. melanogaster: w- / y[1]w[1]; UAS-3xFLAG.dCas9.VPR/Pex5 gRNA O.E.; UAS-Per RNAi/GMR54H02-Gal4	This paper	N/A
D. melanogaster: w- / y[1]w[1]; UAS-3xFLAG.dCas9.VPR/control gRNA; UAS-Per RNAi/GMR54H02-Gal4	This paper	N/A
D. melanogaster: y[1] sc[*] v[1] sev[21]; P{y[+t7.7] v[+t1.8]=GS00089}attP40	BDSC	Cat# 67539; RRID: BDSC_67539
D. melanogaster: y[1] w[*]; P{y[+t7.7] w[+mC]=UAS-3xFLAG.dCas9.VPR}attP40	BDSC	Cat# 66561; RRID: BDSC_66561
D. melanogaster: y[1] w[*]; wg[Sp-1]/CyO; Dr[1]/TM3, Sb[1]	BDSC	Cat# 59967; RRID: BDSC_59967
D. melanogaster: y[1] sc[*] v[1] sev[21]; P{y[+t7.7] v[+t1.8]=TOE.GS01923}attP40	BDSC	Cat# 78666; RRID: BDSC_78666
D. melanogaster: y[1] sc[*] v[1] sev[21]; P{y[+t7.7]v[+t1.8]=TRiP.HMS02045}attP2/TM3, Sb[1]	BDSC	Cat# 40878; RRID: BDSC_40878
D. melanogaster: w[*]; P{w[+mC]=UAS-Clk.Delta}1	BDSC	Cat# 36318; RRID: BDSC_36318
D. melanogaster: w[1118]; P{w[+mC]=UAS-Dcr-2.D}2	BDSC	Cat# 24650; RRID: BDSC_24650
D. melanogaster: w[1118]; PBac{y[+mDint2] GFP[E.3xP3]=vas-Cas9}VK00027	BDSC	Cat# 51324; RRID: BDSC_51324
D. melanogaster: FM7i, P{w[+mC]=ActGFP}JMR3/C(1)DX, y[1] f[1]	BDSC	Cat# 4559; RRID: BDSC_4559
D. melanogaster: y[1] v[1]; P{y[+t7.7] v[+t1.8]=TRiP.HMC04009}attP40	BDSC	Cat# 55322; RRID: BDSC_55322
Other		
BODIPY 493/503 Thermo Fisher Scientific	Thermo	Cat# D3922
Software and algorithms		
ImageJ	FIJI	imagej.net (USA)
Graphpad Prism 10	Graph Pad Software	Subscription ID :2814928

ADODE Illustrator 2020	ADOBE	N/A
Clock Lab Analysis 2	Actimetrrics	N/A
R Studio 2023.12.1 (4.3.1)	R	RRID: SCR_000432

EXPERIMENTAL MODEL AND METHOD DETAILS

Fly Husbandry and Stocks

Drosophila melanogaster were maintained at 25°C, 60% relative humidity and 12-hour light/dark cycle unless specified otherwise. Adults were reared on an agar-based diet consisting of 0.8% cornmeal, 10% sugar, and 2.5% yeast. Fly stocks used in the present

study are mentioned in the above resources table. Female flies (7 days old) were used in lipidomics and confocal experiments, while male flies were used in sleep studies from 6 to 10 days old. Flies and crosses were maintained in plastic vials and bottles in a thermoregulated chamber at 25 degree Celsius following a 12:12 h light-dark cycle with 60% humidity. All experiments were performed 2-3 times independently.

***Pex5.FLAG* knock-in**

The *Pex5.FLAG* knock-in fly was generated using CRISPR/Cas9-mediated homology-directed repair in *Drosophila* (*Figure S2G*). Briefly, the gRNA targeting the 3'-UTR of the *Pex5* locus was cloned into a *pU6-2-chiRNA* vector. The ssODN with 3XFlag sequences flanking with two homology arms was synthesized by Integrated DNA Technologies Inc. The gRNA vector and ssODN were injected into *w1118* flies expressing *vas-Cas9* (BL51324). Injected G0 flies were crossed to an attached-X stock (BL4559) to generate F1 progeny. F1 males carrying the FLAG insertion were identified via PCR and Sanger sequencing, and then crossed with appropriate balancer stocks. The resulting Pex5.FLAG knock-in flies were maintained as stable homozygous stocks.

RNA extraction and quantitative RT-PCR

7–10 female flies were homogenized using TissueLyser II (QIAGEN), and RNA was extracted using TRIzol (Thermo Fisher Scientific). DNase-treated total RNA was then reverse transcribed to cDNA using iScript cDNA Synthesis Kit (Bio-Rad). Quantitative RT-PCR (qRT-PCR) was performed with a Quantstudio 3 Real-Time PCR system and PowerUp SYBR Green Master Mix (Thermo Fisher Scientific). Three independent biological replicates were performed with two technical repeats. The mRNA abundance of each candidate gene was normalized to the expression of RpL32 by the comparative CT methods. Primer sequences are listed in the following: RpL32: forward 5'-CCAGTCGGATCGATATGCTAAG-3′ and reverse 5′-CCGATGTTGGGCATCAGATA-3′; *P*ex5: forward 5′-GATGTGGAGAACCCGTTTGA-3′ and reverse 5′-CGCCACCTCGAAACATAGAA-3′.

Adult Brain Immunohistochemistry

Adult female *Drosophila* (7 days old) were anesthetized on ice. Using Dumont 3C tweezers, brain dissections were immersed and dissected in *Drosophila* Schneider's Media. Brain tissues were immediately fixed in 4% paraformaldehyde (PFA) and kept in a rotator for 25 minutes at room temperature. Subsequently, brains were washed three times for 15 minutes each in 0.2% PBS-TritonX and subsequently kept in blocking solution of 5% normal donkey serum for 1 hour. Tissues were then incubated with primary antibodies for 48 hours overnight at 4°C, followed by three 15 minutes washes of 0.2%PBS-TritonX and then secondary antibody staining for another 48 hours at 4°C. Samples were washed three times for 15 minutes each in 0.2% PBST and then mounted with microfrost slides in Prolong Diamond (Life technologies). Primary antibodies used were as follows: anti-PMP70 (1:200; a gift from Kyu-Sun Lee Lab); anti-ELAV (1:200; DSHB); anti-FLAG(1:200; Thermo); anti-SKL (1:200; a gift from Richard Rachubinski); and anti-nc82 (1:20; DSHB). Secondary antibodies were stained at 1:200 and included 488 donkey anti-mouse, 647 donkey anti-mouse, and 488 anti-guinea Pig (Jackson ImmunoResearch Laboratories Inc, West Grove PA).

Neutral lipid BODIPY 493/503 staining protocol

A 10mM main stock of BODIPY 493/503 was prepared from 10mg of BODIPY 493/503 by adding 5.2mL of DMSO and mixing until l completely dissolved. Working stocks of 2mM were prepared in DMSO and then used 1:100 (final concentration: 20µM) on samples already fixed and stained for primaries and secondaries (see above). Samples were stained with BODIPY 493/503 (20µM) for 10 minutes, before mounting in glycerol and imaging on an Olympus FV3000 confocal as noted above. For BODIPY experiments, ZT2 was exclusively used.

Confocal Microscopy

Images were captured using an Olympus FV3000 laser scanning confocal (Olympus, Waltham, MA, USA). 60x and 100x oil-immersive lens were used to capture brains, with further 5x digital zooms into a consistent cortical region, below the antennal lobes and above the suboesophageal ganglion. 10 slices were taken through the cortex. For the circadian import experiments, acquisition of samples was done blind to genotype by independent investigators in two experimental runs. Multiple ROIs (3-5) of 200 x 200 pixel dimensions were acquired per biological replicate brain.

Image analysis

For Pearson analysis, the *JACoP* plugin tool (*FIJI*) was used to automatically calculate the Pearson correlation coefficient (scale from 0 to 1, with 1 being the highest level of colocalization) between two 16-bit images in different color gradient [112]. For peroxisomal import quantification (SKL and PTS1.YFP), puncta were counted via the cell counter function on FIJI and by blinded independent investigators for 3-5 ROIs of a consistent 200x200 pixel dimension.

For BODIPY lipid droplet analysis, Fiji particle analysis was used to measure lipid droplet size through an automated workflow analysis. Measurements of all replicates of control versus mutant size were plotted in a size difference graph. For lipid droplet total count, multiple ROIs (3-5) of 200 x 200 pixel dimensions were acquired per biological replicate brain to aggregate representative average lipid droplet count of control versus mutant brain samples.

Pex5.FLAG Quantification

Flies of 7 days old age at various timepoints (ZT2/ ZT8/ZT14/ZT20; CT2/CT8) were dissected and fixed (see above, immunohistochemistry). Imaging was conducted on an Olympus FV3000 confocal. Anterior region of the cortex glial cells and surrounding soma below the antennal lobes and above the suboesophageal ganglion were captured using a 60x oil lens (with 5x digital zoom), with 10 slices taken through the cortex of anterior region of brain. 8-bit image were used for analysis by performing thresholding to highlight representative intensity of FLAG staining compared to anti-ELAV stain of the surrounding soma regions. Measurements were taken of intensity to highlight differences in intensity of FLAG regions versus surrounding soma.

Lipidomics extraction and LC-MS/MS

20 female brains at day 7 ZT10-12 were dissected rapidly on ice-cold 1X phosphate-buffer saline and frozen on dry ice in chilled methanol (90% v/v) before storage at -80°C until lipid extraction. A modified folch extraction was used and separate columns and standards were run on an Agilent 6430 Triple Quadrupole. Internal standards used included Equisplash™ LIPIDOMIX®

Quantitative Mass Spec Internal Standard (Avanti #330731) and Oleic Acid-d9 (Avanti #861809), following a protocol similar to [113].

For free fatty acid analysis, an Agilent Zorbax RX-Sil column 3.0 x 100 mm, 1.8 µm particle size was used. The total LC run time was 19 min (with 2.5 min post-run) at a flow rate of 0.3 µL/min. Mobile phase A was composed of isopropanol/hexane/water (58:40:2, v/v) with 5mM ammonium acetate and 0.1% acetic acid. Mobile phase B consisted of isopropanol/hexane/water (50:40:10, v/v) with 5mM ammonium acetate and 0.1% acetic acid. Gradient elution consisted of 0 to 17 min of 0% mobile phase B and an increase from 17 to 18 min until 100% of mobile phase B and after 18 min the mobile phase decreased to 0% for 1 more min. The Agilent 6430 Triple-Quad LC/MS system (Santa Clara, CA) was operated in negative mode. Free fatty acids were identified as $[M - H]^-$ and it was run as a pseudoMRM.

Triglycerides were separate as described by Kehelpannala et al., 2020[114]. An InfinityLab Poroshell 120 EC-C18 2.1 × 100 mm (2.7-Micron particle size) column (Agilent, USA) operated at 55 °C using an Agilent 1260 Infinity LC system (Santa Clara, CA). The solvent system consisted of Mobile phase A acetonitrile (ACN)-water (60:40, v/v) and mobile phase B and isopropanol (IPP)-ACN (90/10, v/v) both containing 10 mM ammonium formate. The gradient was starting with a flow rate of 0.26 mL/min and it was set to first a 0–1.5 min isocratic elution with 32% B which was then increased to 45% B from 1.5 to 4 min, then to 52% B from 4 to 5 min followed by an increase to 58% B from 5 to 8 min. Next, the gradient was increased to 66% B from 8 to 11 min followed by an increase to 70% B from 11 to 14 min and an increase to 75% B from 14 to 18 min. Then, from 18 to 21 min B was increased to 97% and B was maintained at 97% from 21 to 25 min. Finally, solvent B was decreased to 32% from 25 to 25.10 min, and B was maintained at 32% for another 4.9 min for column reequilibration. The Agilent 6430 Triple-Quad LC/MS system (Santa Clara, CA) was operated in positive mode. Triglycerides were identified as $[M + NH4]^+$ molecular ions representing the neutral loss of the fatty acid. The collision voltage was 21 eV.

Gas-phase ions of various lipid species were obtained using electrospray ionization (ESI), with the electrospray needle held at -3,500 V (+) and 3,000 V (–). Data acquisition and analysis was carried out using Agilent Mass Hunter software.

Lipidomic Analysis

Data were analyzed in R studio. Lipids were filtered for abundance across two experimental runs (4 tubes of 20 brains per condition, totaling for controls 8 tubes of *pex5^{KD}* control, 4 tubes of Dcr-2;*repo,* 4 tubes of *Dcr2; nSyb*; and for mutants, 8 tubes of pan-glial *pex5^{KD}*, 8 tubes of neuronal *pex5^{KD}*, and 7 tubes of *CG>pex5^{KD}*). Brains were dissected at ZT10-12. For volcano plots, parent control values were averaged (ie *repo-GAL4* and *pex5^{KD}* were averaged and compared to *repo-GAL4 > pex5^{KD}*). Principal Component Analysis was conducted on sphingolipids, phospholipids, TAG, and free fatty acids using relative % matrices, where the entire lipid composition of a class summed to 100%. Specific ng/brain species plots were analyzed by ANOVA, with Dunnett's test against pex5^{KD} controls, and Benjamini-Hochberg corrected for further genotypic comparisons. For heatmaps, relative abundance was Z-scored per experimental batch and then pooled.

Sleep Behavioral Assay

For sleep behavioral analysis in light-dark conditions (12hr light/12-hr dark), 5-day old post eclosion flies were monitored using *Drosophila* Activity Monitors (DAMs, Trikinetics). Male flies were collected at day 5 of adulthood and loaded into DAMs, then analyzed from

day 6 to day 10 after a 24 hour recovery period. Cessation of activity for 5 mins was used as a proxy for sleep; flies that were inactive for 12h prior to endpoint of the analyzed period were omitted from analysis as dead. For sleep and activity analysis, code was adopted from[113] and analyzed and graphed in R Studio in a batch function agnostic to genotype. Data were also analyzed using ClockLab and Shiny R-DAM (https://karolcichewicz.shinyapps.io/shinyr-dam/). The Mann-Whitney U test was used to test for significant population differences between controls and mutants.

For free-running rhythmicity assay to assess circadian rhythms and endogenous circadian control of peroxisomal import, five day old flies previously entrained in LD were covered with silver aluminum foil and an opaque black cardboard (DD). Immunohistochemistry on DD brains was conducted after 36 hours of DD, while sleep behavior was collected from day 6 to day 10.

Heat Map Hierarchical Clustering & Generation

Code was generated by Anurag Das on PositCloud which replicates JUPYTER notebook environment. Code can be shared upon request. After hierarchical clustering, data were further aggregated and visualized using GraphPad Prism.

QUANTIFICATION AND STATISTICAL ANALYSIS

GraphPad Prism (GraphPad Software Version 10) was used for statistical analysis. Unpaired two-tailed Student's t- test for comparison between 2 groups or one-way ANOVA (Tukey multiple comparison) was performed to compare the mean value between control and treatment groups of more than two groups respectively. Lipidomics data were analyzed and plotted in R studio.

1. Wanders RJA, Baes M, Ribeiro D, Ferdinandusse S, Waterham HR. The physiological functions of human peroxisomes. Physiological Reviews. 2023;103: 957–1024. doi:10.1152/physrev.00051.2021

2. Ding L, Sun W, Balaz M, He A, Klug M, Wieland S, et al. Peroxisomal β-oxidation acts as a sensor for intracellular fatty acids and regulates lipolysis. Nat Metab. 2021;3: 1648–1661. doi:10.1038/s42255-021-00489-2

3. Lodhi IJ, Semenkovich CF. Peroxisomes: a nexus for lipid metabolism and cellular signaling. Cell Metab. 2014;19: 380–392. doi:10.1016/j.cmet.2014.01.002

4. Sodders M, Das A, Bai H. Glial peroxisome dysfunction induces axonal swelling and neuroinflammation in Drosophila. G3 Genes|Genomes|Genetics. 2025;15: jkae243. doi:10.1093/g3journal/jkae243

5. Kassmann CM, Lappe-Siefke C, Baes M, Brügger B, Mildner A, Werner HB, et al. Axonal loss and neuroinflammation caused by peroxisome-deficient oligodendrocytes. Nat Genet. 2007;39: 969–976. doi:10.1038/ng2070

6. Kleinecke S, Richert S, de Hoz L, Brügger B, Kungl T, Asadollahi E, et al. Peroxisomal dysfunctions cause lysosomal storage and axonal Kv1 channel redistribution in peripheral neuropathy. Ackerman SL, editor. eLife. 2017;6: e23332. doi:10.7554/eLife.23332

7. Santos MJ, Henderson SC, Moser AB, Moser HW, Lazarow PB. Peroxisomal ghosts are intracellular structures distinct from lysosomal compartments in Zellweger syndrome: a confocal laser scanning microscopy study. Biol Cell. 2000;92: 85–94. doi:10.1016/s0248-4900(00)89016-4

8. Soliman K, Göttfert F, Rosewich H, Thoms S, Gärtner J. Super-resolution imaging reveals the sub-diffraction phenotype of Zellweger Syndrome ghosts and wild-type peroxisomes. Sci Rep. 2018;8: 7809. doi:10.1038/s41598-018-24119-2

9. Krause C, Rosewich H, Woehler A, Gärtner J. Functional analysis of PEX13 mutation in a Zellweger syndrome spectrum patient reveals novel homooligomerization of PEX13 and its role in human peroxisome biogenesis. Human Molecular Genetics. 2013;22: 3844–3857. doi:10.1093/hmg/ddt238

10. De Munter S, Verheijden S, Régal L, Baes M. Peroxisomal Disorders: A Review on Cerebellar Pathologies. Brain Pathol. 2015;25: 663–678. doi:10.1111/bpa.12290

11. Berger J, Dorninger F, Forss-Petter S, Kunze M. Peroxisomes in brain development and function. Biochim Biophys Acta. 2016;1863: 934–955. doi:10.1016/j.bbamcr.2015.12.005

12. Abe Y, Honsho M, Itoh R, Kawaguchi R, Fujitani M, Fujiwara K, et al. Peroxisome biogenesis deficiency attenuates the BDNF-TrkB pathway-mediated development of the cerebellum. Life Sci Alliance. 2018;1: e201800062. doi:10.26508/lsa.201800062

13. Smith MD, Schnell DJ. Peroxisomal protein import. the paradigm shifts. Cell. 2001;105: 293–296. doi:10.1016/s0092-8674(01)00337-3

14. Dammai V, Subramani S. The human peroxisomal targeting signal receptor, Pex5p, is translocated into the peroxisomal matrix and recycled to the cytosol. Cell. 2001;105: 187–196. doi:10.1016/s0092-8674(01)00310-5

15. Smith JJ, Aitchison JD. Peroxisomes take shape. Nat Rev Mol Cell Biol. 2013;14: 803–817. doi:10.1038/nrm3700

16. Huang K, Miao T, Chang K, Kim J, Kang P, Jiang Q, et al. Impaired peroxisomal import in Drosophila oenocytes causes cardiac dysfunction by inducing upd3 as a peroxikine. Nat Commun. 2020;11: 2943. doi:10.1038/s41467-020-16781-w

17. Bottelbergs A, Verheijden S, Hulshagen L, Gutmann DH, Goebbels S, Nave K-A, et al. Axonal integrity in the absence of functional peroxisomes from projection neurons and astrocytes. Glia. 2010;58: 1532–1543. doi:10.1002/glia.21027

18. Di Cara F, Rachubinski RA, Simmonds AJ. Distinct Roles for Peroxisomal Targeting Signal Receptors Pex5 and Pex7 in Drosophila. Genetics. 2019;211: 141–149. doi:10.1534/genetics.118.301628

19. Coutinho-Budd J, Freeman MR, Ackerman S. Glial Regulation of Circuit Wiring, Firing, and Expiring in the Drosophila Central Nervous System. Cold Spring Harb Perspect Biol. 2024;16: a041347. doi:10.1101/cshperspect.a041347

20. Freeman MR. Drosophila Central Nervous System Glia. Cold Spring Harb Perspect Biol. 2015;7: a020552. doi:10.1101/cshperspect.a020552

21. Kremer MC, Jung C, Batelli S, Rubin GM, Gaul U. The glia of the adult Drosophila nervous system. Glia. 2017;65: 606–638. doi:10.1002/glia.23115

22. Awasaki T, Lai S-L, Ito K, Lee T. Organization and postembryonic development of glial cells in the adult central brain of Drosophila. J Neurosci. 2008;28: 13742–13753. doi:10.1523/JNEUROSCI.4844-08.2008

23. Yildirim K, Petri J, Kottmeier R, Klämbt C. Drosophila glia: Few cell types and many conserved functions. Glia. 2019;67: 5–26. doi:10.1002/glia.23459

24. Hasel P, Liddelow SA. Astrocytes. Current Biology. 2021;31: R326–R327. doi:10.1016/j.cub.2021.01.056

25. Pogodalla N, Winkler B, Klämbt C. Glial Tiling in the Insect Nervous System. Front Cell Neurosci. 2022;16: 825695. doi:10.3389/fncel.2022.825695

26. Kottmeier R, Bittern J, Schoofs A, Scheiwe F, Matzat T, Pankratz M, et al. Wrapping glia regulates neuronal signaling speed and precision in the peripheral nervous system of Drosophila. Nat Commun. 2020;11: 4491. doi:10.1038/s41467-020-18291-1

27. Rey S, Ohm H, Moschref F, Zeuschner D, Praetz M, Klämbt C. Glial-dependent clustering of voltage-gated ion channels in Drosophila precedes myelin formation. Dickman DK, Desplan C, editors. eLife. 2023;12: e85752. doi:10.7554/eLife.85752

28. Birren SJ, Goodrich LV, Segal RA. Satellite Glial Cells: No Longer the Most Overlooked Glia. Cold Spring Harb Perspect Biol. 2025;17: a041367. doi:10.1101/cshperspect.a041367

29. Kunduri G, Turner-Evans D, Konya Y, Izumi Y, Nagashima K, Lockett S, et al. Defective cortex glia plasma membrane structure underlies light-induced epilepsy in cpes mutants. Proc Natl Acad Sci U S A. 2018;115: E8919–E8928. doi:10.1073/pnas.1808463115

30. Melom JE, Littleton JT. Mutation of a NCKX eliminates glial microdomain calcium oscillations and enhances seizure susceptibility. J Neurosci. 2013;33: 1169–1178. doi:10.1523/JNEUROSCI.3920-12.2013

31. Weiss S, Melom JE, Ormerod KG, Zhang YV, Littleton JT. Glial Ca2+signaling links endocytosis to K+ buffering around neuronal somas to regulate excitability. Westbrook GL, Davis GW, Davis GW, Zinn K, editors. eLife. 2019;8: e44186. doi:10.7554/eLife.44186

32. Spéder P, Brand AH. Systemic and local cues drive neural stem cell niche remodelling during neurogenesis in Drosophila. Banerjee U, editor. eLife. 2018;7: e30413. doi:10.7554/eLife.30413

33. Bailey AP, Koster G, Guillermier C, Hirst EMA, MacRae JI, Lechene CP, et al. Antioxidant Role for Lipid Droplets in a Stem Cell Niche of *Drosophila*. Cell. 2015;163: 340–353. doi:10.1016/j.cell.2015.09.020

34. Dubowy C, Sehgal A. Circadian Rhythms and Sleep in Drosophila melanogaster. Genetics. 2017;205: 1373–1397. doi:10.1534/genetics.115.185157

35. Glou EL, Seugnet L, Shaw PJ, Preat T, Goguel V. Circadian Modulation of Consolidated Memory Retrieval Following Sleep Deprivation in Drosophila. Sleep. 2012;35: 1377–1384. doi:10.5665/sleep.2118

36. Chouhan NS, Wolf R, Helfrich-Förster C, Heisenberg M. Flies Remember the Time of Day. Current Biology. 2015;25: 1619–1624. doi:10.1016/j.cub.2015.04.032

37. Hendricks JC, Sehgal A. Why a Fly? Using Drosophila to Understand the Genetics of Circadian Rhythms and Sleep. Sleep. 2004;27: 334–342. doi:10.1093/sleep/27.2.334

38. Allada R, Chung BY. Circadian organization of behavior and physiology in Drosophila. Annu Rev Physiol. 2010;72: 605–624. doi:10.1146/annurev-physiol-021909-135815

39. Cavey M, Collins B, Bertet C, Blau J. Circadian rhythms in neuronal activity propagate through output circuits. Nat Neurosci. 2016;19: 587–595. doi:10.1038/nn.4263

40. Ezagouri S, Asher G. Circadian control of mitochondrial dynamics and functions. Current Opinion in Physiology. 2018;5: 25–29. doi:10.1016/j.cophys.2018.05.008

41. Ng FS, Tangredi MM, Jackson FR. Glial cells physiologically modulate clock neurons and circadian behavior in a calcium-dependent manner. Curr Biol. 2011;21: 625–634. doi:10.1016/j.cub.2011.03.027

42. Rieger D, Shafer OT, Tomioka K, Helfrich-Förster C. Functional Analysis of Circadian Pacemaker Neurons in Drosophila melanogaster. J Neurosci. 2006;26: 2531–2543. doi:10.1523/JNEUROSCI.1234-05.2006

43. Dopp J, Ortega A, Davie K, Poovathingal S, Baz E-S, Liu S. Single-cell transcriptomics reveals that glial cells integrate homeostatic and circadian processes to drive sleep–wake cycles. Nat Neurosci. 2024;27: 359–372. doi:10.1038/s41593-023-01549-4

44. Damulewicz M, Doktór B, Baster Z, Pyza E. The Role of Glia Clocks in the Regulation of Sleep in Drosophila melanogaster. J Neurosci. 2022;42: 6848–6860. doi:10.1523/JNEUROSCI.2340-21.2022

45. Helfrich-Förster C. The period clock gene is expressed in central nervous system neurons which also produce a neuropeptide that reveals the projections of circadian pacemaker cells within the brain of Drosophila melanogaster. Proc Natl Acad Sci USA. 1995;92: 612–616. doi:10.1073/pnas.92.2.612

46. Mazzoni EO, Desplan C, Blau J. Circadian pacemaker neurons transmit and modulate visual information to control a rapid behavioral response. Neuron. 2005;45: 293–300. doi:10.1016/j.neuron.2004.12.038

47. Taghert PH. Circadian Pacemakers: How Clock Properties Relate To Their Cellular Properties. Current Biology. 2011;21: R894–R896. doi:10.1016/j.cub.2011.09.041

143 48. Yu W, Hardin PE. Circadian oscillators of Drosophila and mammals. J Cell Sci.
144 2006;119: 4793–4795. doi:10.1242/jcs.03174

145 49. Ferrarelli LK. Glia are powerhouses for sleep. Science Signaling. 2024;17:
146 eadp9115. doi:10.1126/scisignal.adp9115

147 50. Carvalhas-Almeida C, Sehgal A. Glia: the cellular glue that binds circadian
148 rhythms and sleep. Sleep. 2025;48: zsae314. doi:10.1093/sleep/zsae314

149 51. Chi-Castañeda D, Ortega A. The Role of Mammalian Glial Cells in Circadian
150 Rhythm Regulation. Neural Plasticity. 2017;2017: 8140737.
151 doi:10.1155/2017/8140737

152 52. Neufeld-Cohen A, Robles MS, Aviram R, Manella G, Adamovich Y, Ladeuix B, et
153 al. Circadian control of oscillations in mitochondrial rate-limiting enzymes and
154 nutrient utilization by PERIOD proteins. Proc Natl Acad Sci U S A. 2016;113:
155 E1673-1682. doi:10.1073/pnas.1519650113

156 53. Ezagouri S, Zwighaft Z, Sobel J, Baillieul S, Doutreleau S, Ladeuix B, et al.
157 Physiological and Molecular Dissection of Daily Variance in Exercise Capacity.
158 Cell Metab. 2019;30: 78-91.e4. doi:10.1016/j.cmet.2019.03.012

159 54. Zhang R, Lahens NF, Ballance HI, Hughes ME, Hogenesch JB. A circadian gene
160 expression atlas in mammals: implications for biology and medicine. Proc Natl
161 Acad Sci U S A. 2014;111: 16219–16224. doi:10.1073/pnas.1408886111

162 55. Iascone DM, Zhang X, Brafford P, Mesaros C, Sela Y, Hofbauer S, et al.
163 Hypermetabolic state is associated with circadian rhythm disruption in mouse and
164 human cancer cells. Proceedings of the National Academy of Sciences. 2024;121:
165 e2319782121. doi:10.1073/pnas.2319782121

166 56. Skowyra ML, Feng P, Rapoport TA. Towards solving the mystery of peroxisomal
167 matrix protein import. Trends in Cell Biology. 2024;34: 388–405.
168 doi:10.1016/j.tcb.2023.08.005

169 57. Korotkova D, Borisyuk A, Guihur A, Bardyn M, Kuttler F, Reymond L, et al.
170 Fluorescent fatty acid conjugates for live cell imaging of peroxisomes. Nat
171 Commun. 2024;15: 4314. doi:10.1038/s41467-024-48679-2

172 58. Chung H-L, Wangler MF, Marcogliese PC, Jo J, Ravenscroft TA, Zuo Z, et al.
173 Loss- or Gain-of-Function Mutations in ACOX1 Cause Axonal Loss via Different
174 Mechanisms. Neuron. 2020;106: 589-606.e6. doi:10.1016/j.neuron.2020.02.021

175 59. Yin J, Shao Y, Huang F, Hong Y, Wei W, Jiang C, et al. Peroxisomal membrane
176 protein PMP70 confers drug resistance in colorectal cancer. Cell Death Dis.
177 2025;16: 293. doi:10.1038/s41419-025-07572-6

60. Faust JE, Manisundaram A, Ivanova PT, Milne SB, Summerville JB, Brown HA, et al. Peroxisomes are required for lipid metabolism and muscle function in Drosophila melanogaster. PLoS One. 2014;9: e100213. doi:10.1371/journal.pone.0100213

61. Prolo LM, Takahashi JS, Herzog ED. Circadian Rhythm Generation and Entrainment in Astrocytes. J Neurosci. 2005;25: 404–408. doi:10.1523/JNEUROSCI.4133-04.2005

62. Ewer J, Frisch B, Hamblen-Coyle MJ, Rosbash M, Hall JC. Expression of the period clock gene within different cell types in the brain of Drosophila adults and mosaic analysis of these cells' influence on circadian behavioral rhythms. J Neurosci. 1992;12: 3321–3349. doi:10.1523/JNEUROSCI.12-09-03321.1992

63. Brancaccio M, Edwards MD, Patton AP, Smyllie NJ, Chesham JE, Maywood ES, et al. Cell-autonomous clock of astrocytes drives circadian behavior in mammals. Science. 2019;363: 187–192. doi:10.1126/science.aat4104

64. Lananna BV, Nadarajah CJ, Izumo M, Cedeño MR, Xiong DD, Dimitry J, et al. Cell-Autonomous Regulation of Astrocyte Activation by the Circadian Clock Protein BMAL1. Cell Rep. 2018;25: 1-9.e5. doi:10.1016/j.celrep.2018.09.015

65. Damulewicz M, Doktór B, Baster Z, Pyza E. The Role of Glia Clocks in the Regulation of Sleep in Drosophila melanogaster. J Neurosci. 2022;42: 6848–6860. doi:10.1523/JNEUROSCI.2340-21.2022

66. Tanoue S, Krishnan P, Krishnan B, Dryer SE, Hardin PE. Circadian Clocks in Antennal Neurons Are Necessary and Sufficient for Olfaction Rhythms in Drosophila. Current Biology. 2004;14: 638–649. doi:10.1016/j.cub.2004.04.009

67. Zhang C, Daubnerova I, Jang Y-H, Kondo S, Žitňan D, Kim Y-J. The neuropeptide allatostatin C from clock-associated DN1p neurons generates the circadian rhythm for oogenesis. Proc Natl Acad Sci U S A. 2021;118: e2016878118. doi:10.1073/pnas.2016878118

68. Herrero A, Duhart JM, Ceriani MF. Neuronal and Glial Clocks Underlying Structural Remodeling of Pacemaker Neurons in Drosophila. Front Physiol. 2017;8: 918. doi:10.3389/fphys.2017.00918

69. Riva S, Ceriani MF, Risau-Gusman S, Franco DL. Circadian control of a sex-specific behaviour in Drosophila. eLife. 2024;13. doi:10.7554/eLife.103359.1

70. Ewen-Campen B, Yang-Zhou D, Fernandes VR, González DP, Liu L-P, Tao R, et al. Optimized strategy for in vivo Cas9-activation in Drosophila. Proceedings of the National Academy of Sciences. 2017;114: 9409–9414. doi:10.1073/pnas.1707635114

214 71. Li Y, Haynes P, Zhang SL, Yue Z, Sehgal A. Ecdysone acts through cortex glia to
215 regulate sleep in Drosophila. Ramaswami M, VijayRaghavan K, Keene AC,
216 editors. eLife. 2023;12: e81723. doi:10.7554/eLife.81723

217 72. Haynes PR, Pyfrom ES, Li Y, Stein C, Cuddapah VA, Jacobs JA, et al. A neuron–
218 glia lipid metabolic cycle couples daily sleep to mitochondrial homeostasis. Nat
219 Neurosci. 2024;27: 666–678. doi:10.1038/s41593-023-01568-1

220 73. Ueda K, Anderson-Baron MN, Haskins J, Hughes SC, Simmonds AJ. Recruitment
221 of Peroxin 14 to lipid droplets affects lipid storage in Drosophila. J Cell Sci.
222 2022;135: jcs259092. doi:10.1242/jcs.259092

223 74. Kong J, Ji Y, Jeon YG, Han JS, Han KH, Lee JH, et al. Spatiotemporal contact
224 between peroxisomes and lipid droplets regulates fasting-induced lipolysis via
225 PEX5. Nat Commun. 2020;11: 578. doi:10.1038/s41467-019-14176-0

226 75. Theisen EK, Rivas-Serna IM, Lee RJ, Jay TR, Kunduri G, Nguyen TT, et al. Glia
227 phagocytose neuronal sphingolipids to infiltrate developing synapses. bioRxiv.
228 2025; 2025.04.14.648777. doi:10.1101/2025.04.14.648777

229 76. Carvalho M, Sampaio JL, Palm W, Brankatschk M, Eaton S, Shevchenko A.
230 Effects of diet and development on the Drosophila lipidome. Mol Syst Biol. 2012;8:
231 MSB201229. doi:10.1038/msb.2012.29

232 77. Halassa MM, Fellin T, Takano H, Dong J-H, Haydon PG. Synaptic islands defined
233 by the territory of a single astrocyte. J Neurosci. 2007;27: 6473–6477.
234 doi:10.1523/JNEUROSCI.1419-07.2007

235 78. Allen NJ, Barres BA. Glia — more than just brain glue. Nature. 2009;457: 675–
236 677. doi:10.1038/457675a

237 79. Hanani M. Satellite glial cells in sensory ganglia: from form to function. Brain
238 Research Reviews. 2005;48: 457–476. doi:10.1016/j.brainresrev.2004.09.001

239 80. Takasaki C, Yamasaki M, Uchigashima M, Konno K, Yanagawa Y, Watanabe M.
240 Cytochemical and cytological properties of perineuronal oligodendrocytes in the
241 mouse cortex. Eur J Neurosci. 2010;32: 1326–1336. doi:10.1111/j.1460-
242 9568.2010.07377.x

243 81. Kis V, Barti B, Lippai M, Sass M. Specialized Cortex Glial Cells Accumulate Lipid
244 Droplets in Drosophila melanogaster. PLOS ONE. 2015;10: e0131250.
245 doi:10.1371/journal.pone.0131250

246 82. Silva B, Mantha OL, Schor J, Pascual A, Plaçais P-Y, Pavlowsky A, et al. Glia fuel
247 neurons with locally synthesized ketone bodies to sustain memory under
248 starvation. Nat Metab. 2022;4: 213–224. doi:10.1038/s42255-022-00528-6

83. Buchanan RL, Benzer S. Defective Glia in the Drosophila Brain Degeneration Mutant drop-dead. Neuron. 1993;10: 839–850. doi:10.1016/0896-6273(93)90200-B

84. Dumstrei K, Wang F, Hartenstein V. Role of DE-cadherin in neuroblast proliferation, neural morphogenesis, and axon tract formation in Drosophila larval brain development. J Neurosci. 2003;23: 3325–3335. doi:10.1523/JNEUROSCI.23-08-03325.2003

85. Kremer MC, Jung C, Batelli S, Rubin GM, Gaul U. The glia of the adult Drosophila nervous system. Glia. 2017;65: 606–638. doi:10.1002/glia.23115

86. Schmitt K, Grimm A, Dallmann R, Oettinghaus B, Restelli LM, Witzig M, et al. Circadian Control of DRP1 Activity Regulates Mitochondrial Dynamics and Bioenergetics. Cell Metab. 2018;27: 657-666.e5. doi:10.1016/j.cmet.2018.01.011

87. Maury E, Ramsey KM, Bass J. Circadian rhythms and metabolic syndrome: from experimental genetics to human disease. Circ Res. 2010;106: 447–462. doi:10.1161/CIRCRESAHA.109.208355

88. Chua EC-P, Shui G, Lee IT-G, Lau P, Tan L-C, Yeo S-C, et al. Extensive diversity in circadian regulation of plasma lipids and evidence for different circadian metabolic phenotypes in humans. Proc Natl Acad Sci U S A. 2013;110: 14468–14473. doi:10.1073/pnas.1222647110

89. Amatobi KM, Ozbek-Unal AG, Schäbler S, Deppisch P, Helfrich-Förster C, Mueller MJ, et al. The circadian clock is required for rhythmic lipid transport in Drosophila in interaction with diet and photic condition. J Lipid Res. 2023;64: 100417. doi:10.1016/j.jlr.2023.100417

90. Akhtar RA, Reddy AB, Maywood ES, Clayton JD, King VM, Smith AG, et al. Circadian cycling of the mouse liver transcriptome, as revealed by cDNA microarray, is driven by the suprachiasmatic nucleus. Curr Biol. 2002;12: 540–550. doi:10.1016/s0960-9822(02)00759-5

91. Kita Y, Shiozawa M, Jin W, Majewski RR, Besharse JC, Greene AS, et al. Implications of circadian gene expression in kidney, liver and the effects of fasting on pharmacogenomic studies. Pharmacogenetics. 2002;12: 55–65. doi:10.1097/00008571-200201000-00008

92. McCarthy JJ, Andrews JL, McDearmon EL, Campbell KS, Barber BK, Miller BH, et al. Identification of the circadian transcriptome in adult mouse skeletal muscle. Physiol Genomics. 2007;31: 86–95. doi:10.1152/physiolgenomics.00066.2007

93. Panda S, Antoch MP, Miller BH, Su AI, Schook AB, Straume M, et al. Coordinated transcription of key pathways in the mouse by the circadian clock. Cell. 2002;109: 307–320. doi:10.1016/s0092-8674(02)00722-5

286 94. Reddy AB, Karp NA, Maywood ES, Sage EA, Deery M, O'Neill JS, et al. Circadian
287 orchestration of the hepatic proteome. Curr Biol. 2006;16: 1107–1115.
288 doi:10.1016/j.cub.2006.04.026

289 95. Zvonic S, Ptitsyn AA, Conrad SA, Scott LK, Floyd ZE, Kilroy G, et al.
290 Characterization of peripheral circadian clocks in adipose tissues. Diabetes.
291 2006;55: 962–970. doi:10.2337/diabetes.55.04.06.db05-0873

292 96. Storch K-F, Lipan O, Leykin I, Viswanathan N, Davis FC, Wong WH, et al.
293 Extensive and divergent circadian gene expression in liver and heart. Nature.
294 2002;417: 78–83. doi:10.1038/nature744

295 97. Delventhal R, Barber AF. Sensory integration: Time and temperature regulate fly
296 siesta. Curr Biol. 2022;32: R1020–R1022. doi:10.1016/j.cub.2022.08.072

297 98. Solis BL, Koch R, Nagoshi E. Circadian clock-independent ultradian rhythms in
298 lipid metabolism in the Drosophila fat body. Journal of Biological Chemistry.
299 2025;301. doi:10.1016/j.jbc.2025.110245

300 99. Molusky MM, Ma D, Buelow K, Yin L, Lin JD. Peroxisomal localization and
301 circadian regulation of ubiquitin-specific protease 2. PLoS One. 2012;7: e47970.
302 doi:10.1371/journal.pone.0047970

303 100. Crane DI, Maxwell MA, Paton BC. PEX1 mutations in the Zellweger spectrum of
304 the peroxisome biogenesis disorders. Hum Mutat. 2005;26: 167–175.
305 doi:10.1002/humu.20211

306 101. Krause C, Rosewich H, Woehler A, Gärtner J. Functional analysis of PEX13
307 mutation in a Zellweger syndrome spectrum patient reveals novel
308 homooligomerization of PEX13 and its role in human peroxisome biogenesis.
309 Human Molecular Genetics. 2013;22: 3844–3857. doi:10.1093/hmg/ddt238

310 102. Mast FD, Li J, Virk MK, Hughes SC, Simmonds AJ, Rachubinski RA. A Drosophila
311 model for the Zellweger spectrum of peroxisome biogenesis disorders. Dis Model
312 Mech. 2011;4: 659–672. doi:10.1242/dmm.007419

313 103. Shafer OT, Keene AC. The Regulation of Drosophila Sleep. Curr Biol. 2021;31:
314 R38–R49. doi:10.1016/j.cub.2020.10.082

315 104. Jagannathan SR, Jeans T, Van De Poll MN, van Swinderen B. Multivariate
316 classification of multichannel long-term electrophysiology data identifies different
317 sleep stages in fruit flies. Science Advances. 2024;10: eadj4399.
318 doi:10.1126/sciadv.adj4399

319 105. Sang D, Lin K, Yang Y, Ran G, Li B, Chen C, et al. Prolonged sleep deprivation
320 induces a cytokine-storm-like syndrome in mammals. Cell. 2023;186: 5500-
321 5516.e21. doi:10.1016/j.cell.2023.10.025

106. Guevara C, Li Y, Pyfrom E, Killiany S, Yue Z, Sehgal A. Sleep controls peroxisomal abundance to reduce wake-induced brain oxidation. bioRxiv; 2025. p. 2025.11.28.691144. doi:10.1101/2025.11.28.691144

107. Ding L, Sun W, Balaz M, He A, Klug M, Wieland S, et al. Peroxisomal β-oxidation acts as a sensor for intracellular fatty acids and regulates lipolysis. Nat Metab. 2021;3: 1648–1661. doi:10.1038/s42255-021-00489-2

108. Schulz JG, Laranjeira A, Van Huffel L, Gärtner A, Vilain S, Bastianen J, et al. Glial β-Oxidation regulates Drosophila Energy Metabolism. Sci Rep. 2015;5: 7805. doi:10.1038/srep07805

109. Faust JE, Manisundaram A, Ivanova PT, Milne SB, Summerville JB, Brown HA, et al. Peroxisomes Are Required for Lipid Metabolism and Muscle Function in Drosophila melanogaster. PLOS ONE. 2014;9: e100213. doi:10.1371/journal.pone.0100213

110. Wangler MF, Chao Y-H, Roth M, Welti R, McNew JA. Drosophila models uncover substrate channeling effects on phospholipids and sphingolipids in peroxisomal biogenesis disorders. PLOS ONE. 2025;20: e0324143. doi:10.1371/journal.pone.0324143

111. Martinez M. Abnormal profiles of polyunsaturated fatty acids in the brain, liver, kidney and retina of patients with peroxisomal disorders. Brain Res. 1992;583: 171–182. doi:10.1016/s0006-8993(10)80021-6

112. Bolte S, Cordelières FP. A guided tour into subcellular colocalization analysis in light microscopy. J Microsc. 2006;224: 213–232. doi:10.1111/j.1365-2818.2006.01706.x

113. Vaughen JP, Theisen E, Rivas-Serna IM, Berger AB, Kalakuntla P, Anreiter I, et al. Glial control of sphingolipid levels sculpts diurnal remodeling in a circadian circuit. Neuron. 2022;110: 3186-3205.e7. doi:10.1016/j.neuron.2022.07.016

114. Kehelpannala C, Rupasinghe T, Pasha A, Esteban E, Hennessy T, Bradley D, et al. An Arabidopsis lipid map reveals differences between tissues and dynamic changes throughout development. Plant J. 2021;107: 287–302. doi:10.1111/tpj.15278